

**Design of Soft Knee Exoskeleton and Modeling
Effects of Variable Stiffness for Advanced Space
Suits and Planetary Exploration**

by

Allison Paige Porter

B.S. in Biological Systems Engineering
University of Nebraska-Lincoln, 2017

Submitted to the Department of Aeronautics and Astronautics
in partial fulfillment of the requirements for the degree of

Master of Science in Aeronautics and Astronautics

at the

MASSACHUSETTS INSTITUTE OF TECHNOLOGY

September 2020

© Massachusetts Institute of Technology 2020. All rights reserved.

Author
Department of Aeronautics and Astronautics
August 18, 2020

Certified by
Dava J. Newman
Apollo Professor of Aeronautics and Astronautics
Thesis Supervisor

Accepted by
Zoltan Spakovszky
Professor, Aeronautics and Astronautics
Chair, Graduate Program Committee

Design of Soft Knee Exoskeleton and Modeling Effects of Variable Stiffness for Advanced Space Suits and Planetary Exploration

by

Allison Paige Porter

Submitted to the Department of Aeronautics and Astronautics
on August 18, 2020, in partial fulfillment of the
requirements for the degree of
Master of Science in Aeronautics and Astronautics

Abstract

Existing gas-pressurized space suit designs aim to provide astronauts with a wide range of joint motion while minimizing joint torque during extra-vehicular activity (EVA). However, current space suits have stiff joints with limited range, which impede performance. Future designs should consider that some joint torque can be beneficial in storing elastic energy for locomotion in reduced gravity planetary EVAs. Though current gas-pressurized space suits restrict astronaut movement, they are capable of partially supporting their own mass and storing elastic energy in the lower body, allowing metabolic cost reduction during locomotion in reduced gravity, such as on Mars or the moon. The BioSuitTM developed by the Massachusetts Institute of Technology (MIT), is an advanced, skin-tight compression garment concept, which exerts mechanical counterpressure (MCP) directly on the astronaut's skin with the benefits of increasing range of motion and performance while also reducing mass when compared to gas-pressurized space suits. A BioSuitTM soft knee exoskeleton with tunable knee stiffness was developed to minimize metabolic expenditure during locomotion in partial gravity and maximize mobility. Musculoskeletal modeling simulated predicted soft knee exoskeleton stiffness at the knee during walking in Earth and Lunar gravity. This thesis summarizes the design and development of prototype actuation in a soft exoskeleton in collaboration with the D-Air Lab (Vicenza, Italy) that applies variable knee stiffness. Soft knee exoskeleton design criteria, fabrication techniques, and simulated impacts on joint kinematics and metabolic cost are discussed. The soft knee exoskeleton was shown to exert tunable knee stiffness via airbags. Prototypes were developed to minimize partial gravity locomotion metabolic cost and space suit inflexibility. An OpenSim software pipeline was shown to be capable of torsional spring stiffness modeling at the knee analogous with predicted soft knee exoskeleton stiffness. Integration of 1G and 0.17G walking data enabled comparison of energetics trends between exoskeleton conditions within each gravity level. The results of this thesis demonstrate the ability to integrate a soft knee exoskeleton into the BioSuitTM

to improve space suit design and enable longer, safer, and more complex EVAs in partial gravity.

Thesis Supervisor: Dava J. Newman

Title: Apollo Professor of Aeronautics and Astronautics

Acknowledgments

Just as astronauts could not perform a complex EVA without support from the Mission Control Center, I could not have completed this thesis without assistance and encouragement from my extensive support system.

Dava Newman, thank you for your valuable advice and guidance. Over the last two years, I have been so impressed and inspired by your ability to identify the precise piece of information or contact that would overcome my current research hurdle, then provide an immediate connection. Thank you for helping me navigate my way into graduate education at MIT from my very first day as your student. Your experience and renown in bioastronautics is unparalleled, and I am so grateful to have you as my mentor.

The Human Systems Lab became my MIT home, due largely to my fellow lab mates. Rachel, Becca, Jeremy, Alvin, Ferrous, Shea, Golda, and Maya, thank you for being such a wonderful cohort. I couldn't have asked for a better group of people to welcome me into grad school. Marc, I appreciate your feedback and advice regarding my late-night OpenSim issues! Of course, I owe a huge thank you to the HSL staff, including Raina Puels, Liz Zotos, and Quentin Alexander, without whom the lab would not be able to function.

One completely unexpected experience that resulted from the last two years was my summer spent in Vicenza, Italy, working on my soft knee exoskeleton prototype - I can't thank Vittorio Cafaggi, Irina Potryasilova, Enroco Rossetto, Alessandro Guzzon, Barnaba Marchesini, and Barbara De Boni at the D-Air Lab enough. Not only were you vital in design and fabrication of the prototypes, but you also ensured my time in Italy was well spent eating the best food and visiting the most spectacular sights. Grazie!

I would not have been able to complete the entire second aim of my thesis had it not been for the folks in the NASA Johnson Space Center Anthropometry & Biomechanics Facility. Liz Benson, Linh Vu, and Sudhakar Rajulu, I appreciate your quick responses to my emails and rush to ensure I had access to partial gravity ambulation data.

That was probably record time that I've seen something be processed through export control!

To the DoD National Defense Science and Engineering Graduate fellowship office, thank you for your confidence in me and funding my work. Jason Pusey, you have been a great NDSEG mentor and helped provide me with new troubleshooting ideas and inspiration. I look forward to continuing our collaboration through my Ph.D.

I cannot overstate how large a role my family and close friends played in my move to Cambridge and MIT. Mom and Dad, you have never failed to tell me how proud of me you are, through many graduations, internships, and moves between cities. Your house will always be my home. I couldn't have done this without you.

I can always count on my sisters, Ashley and Sydney, to guarantee that I make some time for fun on my trips back to Nebraska. Alexa, you are probably the only person in the world who I would travel halfway across the country to help celebrate your wedding as Maid of Honor a week before my thesis was due! Rachel and Neha, our many apartment wine and movie nights always provide such a lovely getaway from research and classes. Jordan, you deserve a medal for the unwavering optimism and reassurances through not only this thesis, but through the entire last 7 years together. I love you all!

The endless support by this outstanding group of people was vital in my success, especially during the COVID-19 global pandemic that caused me (and many others) to make some last minute shifts in plan and schedule. If I recounted every kind gesture, word of encouragement, and listening ear that was provided to me by all of the individuals listed above (and likely more that I failed to mention), I could write a second 100+ page document. I'm sure I will not be able to repay you all, but you have my sincerest and grandest "thank you" for helping me chase my dreams to help advance human spaceflight.

Contents

1	Introduction	19
1.1	Motivation	19
1.2	Problem Statement and Specific Aims	21
1.3	Hypotheses	22
1.3.1	Hypothesis 1	22
1.3.2	Hypothesis 2	22
1.4	Contributions	22
1.5	Roadmap to Thesis	23
2	Literature Review	27
2.1	Extravehicular Activity (EVA)	27
2.1.1	Gas-Pressure Suit Development	27
2.1.2	Astronaut Physiology and Performance in Reduced Gravity	33
2.2	Mechanical Counterpressure (MCP)	35
2.2.1	MCP vs. Gas-Pressure Suits	36
2.2.2	Space Activity Suit	36
2.2.3	BioSuit™	37
2.2.4	Lines of Non-Extension (LoNE)	39
2.3	Exoskeleton Mechanics	41
2.3.1	Gait Overview	41
2.3.2	Exoskeleton and Space Suit Energetics	42
2.3.3	Tuned Knee Stiffness Biomechanics	44

2.3.4	Lower-Body Soft Exoskeleton Actuation and Metabolic Cost Impacts	46
2.3.5	Musculoskeletal Modeling for Spaceflight	48
2.3.6	Summary of Literature	50
3	Methods and Prototyping	51
3.1	Soft Knee Exoskeleton Design Criteria	51
3.2	Fabrication Techniques	52
3.2.1	WholeGarment Knitting	52
3.2.2	Airbag Fabrication	56
3.2.3	Preliminary Airbag Characterization	67
3.3	Modeling in OpenSim	68
3.3.1	OpenSim Lower Body Extremity Model	68
3.3.2	Soft Knee Exoskeleton Stiffness and Model Integration	71
3.3.3	Unassisted vs. Assisted Simulated Walking in 1G	73
3.3.4	Unassisted vs. Assisted Walking in Partial Gravity	75
4	Results	81
4.1	Final Soft Knee Exoskeleton Prototype	81
4.2	Modeled Knee Stiffness in 1G and 0.17G	83
4.2.1	Joint Kinematics and Moments in 1G and 0.17G	83
4.2.2	Muscle-Driven Model Comparison to Unassisted Walking Model	85
4.2.3	Test Condition Peak Values	88
5	Discussion	89
5.1	Contributions	90
5.1.1	Hypothesis and Specific Aim 1	90
5.1.2	Hypothesis and Specific Aim 2	92
5.2	Challenges and Limitations	94
5.3	Future Work	96
5.4	Conclusions	98

A Appendix: Soft Knee Design and Fabrication	99
B Appendix: OpenSim Modeling	103

List of Figures

2-1	A) Berkut suit worn by Leonov. Image credit: (Thomas, 2016)) B) Cutout of Gemini 4 EVA suit, worn by Ed White in 1965 Image credit: (Thomas, 2016). C) NASA astronaut Buzz Aldrin wearing the Apollo era EVA suit on the moon’s surface. Image credit: (NASA, 2013). D) The assembly of the Orlan. Image credit: (Skoog & Abramov, 1986). E) NASA Astronaut Jeff Williams wearing the EMU during a 2006 ISS EVA. Image credit: (NASA, 2014).	30
2-2	Components of Shuttle EMU. Image credit: (McMann & McBarron, 1985).	30
2-3	Layers of EMU. Image credit: (NASA, n.d.).	31
2-4	Comparison of features between the xEMU Lite and xEMU intended for future planetary missions. Image credit: (Rodriggs, 2017).	32
2-5	A) NASA Z-2 prototype. Image credit: (McFarland, 2016). B) NASA xEMU ground prototype. Image credit: NASA.	32
2-6	A) Knee joint EMU torques across a spectrum of flexion angles, measured in an empty suit joint. Data collected by Schmidt (blue) and Dionne (red) (P. Schmidt, Newman, & Hodgson, 2001), (Dionne, 1991). Image credit: (P. Schmidt et al., 2001).	35
2-7	1971 Space Activity Suit developed by Webb and Annis. Image credit: (Annis & Webb, 2004).	37
2-8	Conceptual renderings of a conformal helmet and modular portable life support system for the BioSuit™ created by Michal Kracik (Kracik, Meyen, Trotti, & Newman, 2012).	38

2-9	BioSuit™ illustrations and mock-ups with lines of non-extension patterning. Center image credit: Jeremy Stroming (Stroming, 2020). Left and right image credit: Dava Newman.	39
2-10	Strain measurement contributions from Iberall, Bethke, Wessendorf, and Newman to LoNE calculation for the mockup of the BioSuit™. Adapted from (Iberall, 1964), (Newman & Wessendorf, 2015), (Wessendorf & Newman, 2012), (Obropta & Newman, 2015), and (Dainese, 2019).	40
2-11	Phases of human gait cycle. Image credit: (McMahon, 1984).	41
2-12	Exoskeleton (left) and fiberglass legs (right). Image credit: (Carr & Newman, 2008).	43
2-13	Proposed non-linear relationship between specific resistance with relative leg stiffness (where k represents stiffness). Image credit: (Carr & Newman, 2017).	43
2-14	Spring-mass model of leg stiffness interaction with a surface. Image credit: (Carr & Newman, 2017).	44
2-15	Soft exosuit utilizing pneumatic actuators. Image credit: (Wehner et al., 2013).	47
2-16	Soft exosuit utilizing Bowden cables. Image credit: (Lee et al., 2018).	47
3-1	MCP calculation where P is pressure, R is limb radius, t is fabric thickness, and σ_h is hoop stress exerted by fabric (Obropta, 2015) . .	53
3-2	First iteration of WholeGarment-knitted sleeves	54
3-3	Second iteration of WholeGarment knitted sleeves.	54
3-4	Second iteration of WholeGarment knitted sleeves placed on mannequin arms.	55
3-5	Final base fabric prototype (left) placed on a mannequin arm (right).	55
3-6	Knee joint rotation during flexion and extension (image adapted from (NASM, 2015)).	56
3-7	Conceptual airbag (green) configuration design (image adapted from (NASM, 2015)).	57

3-8	A) Shima Seiki SWG 091N machine was employed for WholeGarment knitting of integrated airbag and knee sleeve. B) Base fabric sleeve. C) Deflated (top) and inflated (bottom) example of airbag integrated into sleeve base material. D) CAD diagram of airbag orientation and measurements in mm. E) WholeGarment-knitted soft knee exoskeleton sleeve without lamination. F) Final soft knee exoskeleton with laminated airbags. (Porter, Marchesini, Potryasilova, Rossetto, & Newman, 2020).	58
3-9	Base fabric and inflated airbag (left) and deflated airbag (right). . . .	59
3-10	Sketch of knee airbag structure, dimensions in mm.	60
3-11	Anterior (left), lateral (center), and posterior (right) views of soft knee exoskeleton V1 with insufficient elasticity of base fabric separating posterior airbags (circled).	60
3-12	Soft knee exoskeleton V2 anterior (left) and posterior (right) views. . .	61
3-13	Soft knee exoskeleton V2 donned (left) and maximally inflated (right). A) Anterior view. B) Lateral view.	62
3-14	Soft knee exoskeleton V3 donned and maximally inflated anterior (left) and lateral (right) views.	63
3-15	Model strain field (left) and rendering (right). Deflated A) Lateral view. B) Anterior view. C) posterior view. Green = lowest strain, red = highest strain.	64
3-16	Model strain field (left) and rendering (right). Inflated A) Lateral view. B) Anterior view. C) posterior view. Green = lowest strain, red = highest strain.	65
3-17	linear relationship between soft knee exoskeleton and mechanical leg model flexion angle (α) and moment (M_y). The slope represents system stiffness (K).	67
3-18	Delp et al. sagittal plane geometries. Image Credit: (Delp et al., 1990).	70
3-19	OpenSim gait pipeline.	71

3-20	Simple diagram of a torsional spring with a deflection force (F) applied from a distance between the force and the spring center (L) to create a moment.	72
3-21	OpenSim gait pipeline for 1G condition.	74
3-22	Muscles associated with knee extension (blue) and knee flexion (red) included in the OpenSim2392 model. Images adapted from: (H.Gray, 1913).	75
3-23	A subject performing a treadmill locomotion task using the POGO partial gravity simulator during an EVA study (NASA, 2020).	76
3-24	Gait2392 model with experimental markers (pink) aligning with NASA POGO trials.	78
3-25	OpenSim gait pipeline for 0.17G condition.	79
4-1	Soft knee exoskeleton V2 donned and maximally inflated anterior (left) and lateral (right) views.	82
4-2	Soft knee exoskeleton V3 donned and maximally inflated anterior (left) and lateral (right) views.	83
4-3	OpenSim gait pipeline for 1G condition.	84
4-4	OpenSim gait pipeline for 0.17G condition with removed tool steps (Inverse Dynamics and RRA) and model outputs (Net joint reaction force and moments) that could not be performed with available GRF data.	84
4-5	A) Knee and B) ankle joint angles resulting from inverse kinematics of 1G and 0.17G marker trajectories.	85
4-6	Knee moment resulting from inverse dynamics of 1G GRF and marker trajectory data.	86
4-7	A) Knee Flexion and B) Knee Extension actuation force for Unassisted, Exo 1, Exo 2, and Exo 3 during 1G walking. Actuation force is normalized relative to the Unassisted condition.	86

4-8	2010 Umberger Metabolic Probe analysis in Unassisted, Exo 1, Exo 2, and Exo 3 conditions for A) Knee Flexion, B) Knee Extension, and C) Total Body muscle groups in 1G. Metabolic cost is normalized relative to the Unassisted condition.	87
4-9	2010 Umberger Metabolic Probe analysis in Unassisted, Exo 1, Exo 2, and Exo 3 conditions for A) Knee Flexion, B) Knee Extension, and C) Total Body muscle groups in 0.17G. Metabolic cost is normalized relative to the Unassisted condition.	87
A-1	CAD drawing of soft knee exoskeleton prototype V3 (dimensions in inches).	102

List of Tables

3.1	Anterior, Lateral, and Posterior views of Prototypes V1, V2, and V3 in donned/doffed and inflated/deflated conditions.	66
3.2	Preliminary stiffness value and maximum torque at 45 degrees for each soft knee exoskeleton inflated pressure. Adapted from D-Air Lab measured results.	68
3.3	Defined parameters for torsional spring model simulation conditions. .	73
4.1	Preliminary stiffness value and maximum torque at 45 degrees for each soft knee exoskeleton inflated pressure. Adapted from D Air Lab measured results.	82
4.2	Peak moment, metabolic cost, and actuation force values for Exo 1, 2, and Exo 3 during A) 1G and B) 0.17G. Each value is normalized relative to the Unassisted case in the corresponding gravity level. . .	88
A.1	Leferon (Barcelona, Spain) technical data sheet for PA 6 78/24/2 polyamide yarn.	100
A.2	Expotex (Stezzano, Italy) technical data sheet for CY 325-156 TP/Nylon thermoplastic coated yarn.	101
B.1	Muscles present in the Gait2392 model. All muscles listed are included for both the left and right sides of the model.	104

Chapter 1

Introduction

1.1 Motivation

In 2019, the National Aeronautics and Space Administration (NASA) celebrated the 50th anniversary of the Apollo 11 astronauts first placing human foot prints on lunar soil. July 21, 1969 represents a landmark of exploration - a day when the human desire to seek adventure and satiate our curious nature overcame the countless obstacles and challenges posed by the notion of landing on the moon.

Though the moon has not seen human presence since 1972, NASA has set out to return to lunar surface by 2024, known as the Artemis mission, as the first step toward realizing the Mars Exploration Program. In order to carry out the Artemis mission, space suit technology advancement for use in partial gravity must be a priority. The Apollo space suit was metabolically expensive and significantly restricted the user's range of motion, nearly preventing astronauts from recovering from falls on the moon. In order to perform geological surveys, traverse rough and uneven terrain, conduct planetary science experiments, and construct and maintain habitats, space suits must enable free locomotion and ease of movement during extravehicular activity (EVA). Furthermore, soft exoskeleton technology has the potential to augment astronaut performance in order to conserve metabolic expenditure in partial gravity without the cumbersome mass associated with rigid exoskeletons.

Existing gas-pressurized space suit designs aim to provide astronauts with a wide

range of joint motion while minimizing joint torque during extra-vehicular activity. However, current space suits have limited joint range and stiff knee and elbow joints, which impedes performance. Future designs should consider that some joint torque can be beneficial in storing elastic energy for locomotion in reduced gravity planetary EVAs. Carr and Newman postulated that though current space suits restrict astronaut movement, they are capable of partially supporting their own weight and storing elastic energy in the lower body, which may allow metabolic cost reduction during transport in reduced gravity, such as on Mars or the moon (Carr & Newman, 2017). Though tuned knee stiffness may optimize metabolic cost expenditure, there is limited understanding of how tuned joint stiffness could impact gait kinematics in earth gravity, as well as reduced gravity. Additionally, it is not clear what magnitude of stiffness is required in different gravity environments is optimal in reducing metabolic cost associated with ambulation. Investigation of the effect of variable knee joint stiffness on gait in varying gravity levels could inform the next generation of space suit design and EVA planning.

The BioSuitTM, developed by the Massachusetts Institute of Technology (MIT), is a promising example of such a next-generation space suit. The BioSuitTM is an advanced, skin-tight compression garment concept, which exerts mechanical counter-pressure (MCP) directly on the astronaut’s skin with the benefits of increasing motion and performance and reducing mass as compared to gas-pressurized space suits (Newman, Canina, & Trotti, 2007). The soft exoskeleton development described in this thesis will aid in enabling the BioSuitTM to exert tunable knee-joint stiffness to minimize metabolic expenditure during locomotion in partial gravity, as well as maximize mobility and enhance performance of astronauts. An OpenSim musculoskeletal modeling method is outlined that can help predict joint kinematics, dynamics, and muscle metabolic cost in varying gravity levels and exoskeleton conditions.

In 1962, President John F. Kennedy rallied a nation by declaring “we choose to go to the Moon”. Scientists and engineers worked diligently to provide safe, novel technology to accomplish this feat; over 50 years later, we continue to channel President Kennedy’s sense of adventure and perseverance by setting our sights on Mars.

1.2 Problem Statement and Specific Aims

The main goal of this thesis is to develop and evaluate prototype actuators in a soft exoskeleton that can apply adjustable stiffness to the knee while permitting full range of motion for flexion and extension. Additionally, the fabrication method of this sleeve must include the capability to aid in producing sufficient mechanical counterpressure for safe use in space. Computational modeling may be a useful tool to perform quick and inexpensive simulations to evaluate the efficacy of the soft knee exoskeleton in varying gravity environments.

Development of these prototypes is important to maximize locomotion in reduced gravity while minimizing metabolic cost expenditure associated with locomotion and space suit inflexibility. The integration of exoskeleton sleeves into the BioSuit™ will inform future space suit design to enable longer, safer, and more complex EVAs in partial gravity.

In order to pursue the goal of developing and assessing the performance of tuned knee stiffness and predicting metabolic cost impacts in partial gravity, emphasis was placed on the following two research aims:

- Specific Aim 1: Develop a prototype soft exoskeleton tunable knee stiffening sleeve.
- Specific Aim 2: Investigate the impact of varied stiffness prescription on locomotion mechanics and metabolic consumption in Earth and Lunar gravity using computational simulation of walking.

Computational modeling can be leveraged to evaluate the efficacy of tuned joint stiffness in partial gravity in a way that minimizes experimental time and financial expenses, leading to more efficient design and fabrication of a soft knee exoskeleton for use in space suits and EVAs. By developing a robust and novel soft knee exoskeleton that has tuned joint stiffness capabilities, this work seeks to help reduce required life-support consumables, enable excursions that traverse longer distances and varying terrain, maintain safety, and augment the performance of astronauts.

1.3 Hypotheses

Two hypotheses were proposed with respect to each Specific Aim described in Section 1.2:

1.3.1 Hypothesis 1

WholeGarment knitting can be employed to develop a prototype tunable knee stiffening sleeve and provide hoop stress to provide MCP. This fabrication method will also provide future integration of LoNE patterning. Integrated airbag technology can exert a range of stiffness which provides varying opposition to flexion during locomotion.

1.3.2 Hypothesis 2

A soft knee exoskeleton can be modeled as a torsional spring stiffness at the knee via OpenSim software (Stanford, Palo Alto, CA). Gait mechanics, muscle forces, and estimated muscle metabolic expenditure can be compared between unassisted walking and assisted walking with an exoskeleton in Earth and Lunar gravity using the OpenSim pipeline. Variable knee joint stiffness in an exoskeleton can allow for reduced metabolic cost in select gravity conditions during walking musculoskeletal model simulations.

1.4 Contributions

This research contributes to the fields of soft exoskeletons, space suit design, musculoskeletal modeling, and astronaut locomotion energetics. Prototype soft exoskeletons were developed, in collaboration with the Dainese D-Air Lab, that are able to exert stiffness to the knee while permitting full knee flexion and extension mobility. Additionally, this sleeve demonstrates the capability of WholeGarment knitting to aid in producing sufficient MCP for safe use in space. Design criteria and fabrication techniques are discussed. These prototype sleeves were developed to investigate the

cost-benefit of energy storage in knee stiffness versus the metabolic cost of joint stiffness due to hindrance of user movement.

OpenSim capabilities enable torsional spring stiffness modeling at the knee analogous with predicted stiffness behavior of the soft knee exoskeleton. The chosen method of this stiffness modeling enables specification of upper and lower torsional spring stiffness, upper and lower joint angle limit, damping and transition terms. Integration of OpenSim sample walking data for 1G and NASA experimental Lunar gravity walking data provided the ability to compare calculated joint angles, joint moments, muscle actuation force, and metabolic expenditure between exoskeleton conditions within each gravity level.

The results of this work demonstrate the ability to integrate soft exoskeleton sleeves into the BioSuitTM to improve space suit design to enhance astronaut performance during EVAs in partial gravity. A musculoskeletal modeling pipeline was demonstrated that can predict estimated metabolic cost trends in varying soft exoskeleton stiffness conditions. These results also further aid in understanding how modeled knee stiffness impacts simulated locomotion regulation in order to increase the metabolic efficiency of astronauts during EVAs.

1.5 Roadmap to Thesis

Chapter 1: Introduction - This chapter introduces the research problems motivating this thesis, as well as the proposed solutions to these challenges. Chapter 1 also provides a framework to the content and structure of this thesis.

Chapter 2: Literature Review - Chapter 2 provides an overview of EVA, traditional gas-pressure space suits, astronaut performance, and spaceflight musculoskeletal modeling. This chapter also discusses the prior work related to MCP and soft exoskeletons, providing context to the significance of investigating the relationship between leg stiffness, mobility, and physiology.

Chapter 3: Methods - This chapter describes design criteria and fabrication techniques for the prototype knee soft knee exoskeleton. WholeGarment knitting was

implemented to build knee stiffening air bags. Soft knee exoskeleton design was iterated to produce three prototypes. OpenSim exoskeleton and musculoskeletal modeling methodology is described. The Gait2932 lower-body model and sample walking data were leveraged to generate a muscle-driven simulation with a knee spring with stiffness analogous to the soft knee exoskeleton. Exoskeleton conditions were modeled by specifying upper and lower torsional spring stiffness, upper and lower joint angle limit, damping and transition terms

Chapter 4: Results - The final design of the prototype knee exoskeleton is reported. A process was developed for producing three iterations of a soft exoskeleton knee sleeve prototype that can contribute to MCP. As the airbags are maximally inflated, stiffness in parallel to the knee is exerted. Preliminary stiffness characterization results are listed. Simulated metabolic cost and kinematic analysis are conducted and presented resulting from varying knee sleeve stiffness conditions. An OpenSim software pipeline was shown to be capable of torsional spring stiffness modeling at the knee analogous with predicted soft knee exoskeleton stiffness. Integration of 1G and 0.17G walking data enabled comparison of energetics trends between exoskeleton conditions within each gravity level.

Chapter 5: Discussion - This chapter reviews the research that is presented in this thesis. The results of Chapter 4 are related to the initial hypotheses and Specific Aims discussed in Chapter 1. Design and fabrication of a soft knee exoskeleton that can apply adjustable stiffness to the knee while permitting full range of motion for flexion and extension was demonstrated. OpenSim software capabilities enabled torsional spring stiffness modeling at the knee analogous with predicted stiffness behavior of the soft knee exoskeleton, demonstrating a promising methodology for quickly simulating joint angles, joint moments, muscle actuation force, and metabolic expenditure conditions across a gravity spectrum. Computational simulation results depict a general downward trend in 0.17G knee extension and total body metabolic cost in the Exo conditions as stiffness increased, suggesting that higher magnitudes of stiffness at the knee exerted by a soft knee exoskeleton could continue to decrease these metabolic values. If so, further increase in knee exoskeleton stiffness could result in a decreased

metabolic cost of knee extension and total body in Lunar gravity. Limitations of this thesis and future work are also addressed and the overarching takeaways of this thesis are reiterated.

Chapter 2

Literature Review

2.1 Extravehicular Activity (EVA)

Extravehicular Activity (EVA), commonly referred to as “spacewalks”, enable astronauts to conduct a diverse variety of missions outside of the spacecraft. One of the technical challenges of EVA is due to the adaptation of human physiology to operate under one atmosphere of pressure, or 103.3 kPa. Since our bodies have evolved to nominally operate in such conditions, EVA suits must be designed in a manner which enables regulation of physiological process in space that would normally occur at this atmospheric pressure.

Planetary EVA could include retrieving surface samples, surveying nearby terrain, and attending to the maintenance of the space craft. These activities can involve complex movements and require hours of labor. Therefore, EVA suits must not only protect the astronaut against depressurization, solar radiation, temperature fluctuation, micrometeorites, and dust, but they also need to provide the astronaut with the freedom of movement to perform such tasks without becoming fatigued.

2.1.1 Gas-Pressure Suit Development

The design of suits intended for Intravehicular Activity (IVA) and EVA were inspired by pressure suits worn in aviation, which were used as a countermeasure the low

pressures achieved by high altitude flight. IVA suits included the Soviet SK-1 and the Mercury suit developed by NASA, but did not adequately protect the user from the anticipated microgravity of EVA (Anderson, 2011). Therefore, both the Soviet space agency and NASA began designing their respective EVA suit technology.

The first pressurized space suit that was utilized during an EVA was the Soviet Berkut suit, shown in Figure 2-1A and worn by Alexi Leonov during the world's first EVA in 1965 (Thomas, 2016).

The Berkut had a nominal pressurization of 40 kPa and consisted of an inner double pressure bladder layer, a Kapron restraint layer, and a protective outer covering. Its purpose was to enable a single crew member to conduct an EVA, or rescue two crewmembers in the case of spacecraft depressurization (Thomas, 2016). This suit was only designed for 45 minutes of continuous use in microgravity and provided consumables to the user via an umbilical. Leonov returned to the airlock of the spacecraft after the 22 minutes of pressurization time; however, pressurization of the suit resulted in ballooning, rigidity, and mobility problems and he required assistance to re-enter the airlock (Skoog, Abramov, Stoklitsky, & Doodnik, 2002). These difficulties exposed extreme mobility issues associated with suit pressurization.

In response to Leonov's historic accomplishment in conducting an EVA, NASA also developed its first EVA suit, the Gemini IV shown in Figure 2-1B. The maximum usage time for the Gemini IV was 36 minutes, and was worn by Ed White in 1965 for his 20-minute EVA. The suit contained pressure bladder and restraint layers, similarly to the Berkut, but also had a bumper layer, aluminized thermal layer, felt layer, and outer covering. Oxygen, bioinstrumentation, and tethering to the capsule was provided to the astronaut using an umbilical (Johnston, 1967). Users of the Gemini and Berkut suits experiences limitations in mobility, as well as insufficient cooling as the users expended significant metabolic work in maneuvering within the suits (Waldie, 2005a).

Though the Gemini and Berkut suits were successful in maintaining the safety of the NASA and Soviet crew, sights were set on the moon and the need arose for a new, mobile generation of space suit which would enable lunar locomotion and exploration.

The two design objectives for the Apollo space suit included the ability to perform up to four hours of lunar EVA and providing mobility within the command module while wearing the suit (Johnston, 1967). Gravity on the moon is about 1/6 that of Earth's gravity (0.17G) and the Apollo suit, shown in Figure 2-1C, was designed to maintain a 3.7 psia pressure level with 100% oxygen.

The umbilical would be removed in order to provide mobility to the system and thermal regulation would be supplemented by the addition of a liquid cooling garment. The Apollo suit, as well as the new Soviet Orlan suit (Figure 2-1D), transitioned from completely soft EVA suits to semi-rigid suits with a stiff torso unit to prevent the problematic ballooning that was experienced in the Gemini and Berkut suits (Waldie, 2005b). Unfortunately, astronauts wearing these suits continued to have severe leg and hip-joint mobility limitations. These limitations were concerning, but since manned missions to the moon concluded in 1972 with Apollo 17, EVA was constrained to microgravity in low-earth orbit for the foreseeable future. Therefore, hip and leg mobility for ease of locomotion was no longer a primary concern.

While the Orlan suit has continued to be used by the Russian Space Agency to present date, NASA developed the Extravehicular Mobility Unit (EMU) in 1982 for use in the Space Shuttle and International Space Station (ISS) missions, and is still used on the ISS today. The EMU is shown in Figure 2-1E.

The EMU was designed following the Apollo missions with the goals to improve the operational capabilities of astronauts during EVA and to be used for multiple missions by male and female astronauts (McMann & McBarron, 1985). In order to redesign the EMU, the suit was no longer required to maintain compatibility with the life support systems onboard the orbiter, enabling the design to be focused on EVA operation only and allowing for a novel primary life support system (PLSS) (McMann & McBarron, 1985). Additionally, the mobility of the astronaut's upper body was prioritized for the EMU, since its primary operational environment would be the Shuttle, and later the ISS. Due to its intended use in microgravity, rather than partial gravity, there was no effort to include lower body mobility (McMann & McBarron, 1985). Each component of the Shuttle EMU is shown in Figure 2-2.

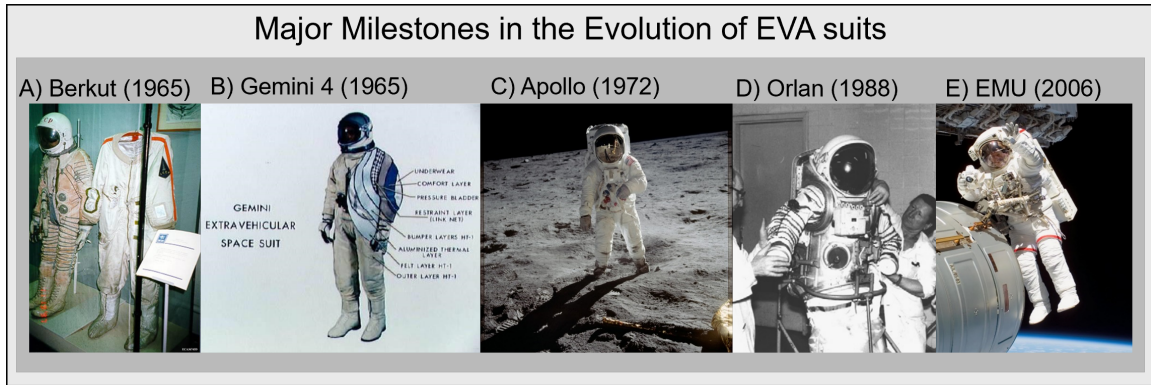


Figure 2-1: A) Berkut suit worn by Leonov. Image credit: (Thomas, 2016)) B) Cutout of Gemini 4 EVA suit, worn by Ed White in 1965 Image credit: (Thomas, 2016). C) NASA astronaut Buzz Aldrin wearing the Apollo era EVA suit on the moon’s surface. Image credit: (NASA, 2013). D) The assembly of the Orlan. Image credit: (Skoog & Abramov, 1986). E) NASA Astronaut Jeff Williams wearing the EMU during a 2006 ISS EVA. Image credit: (NASA, 2014).

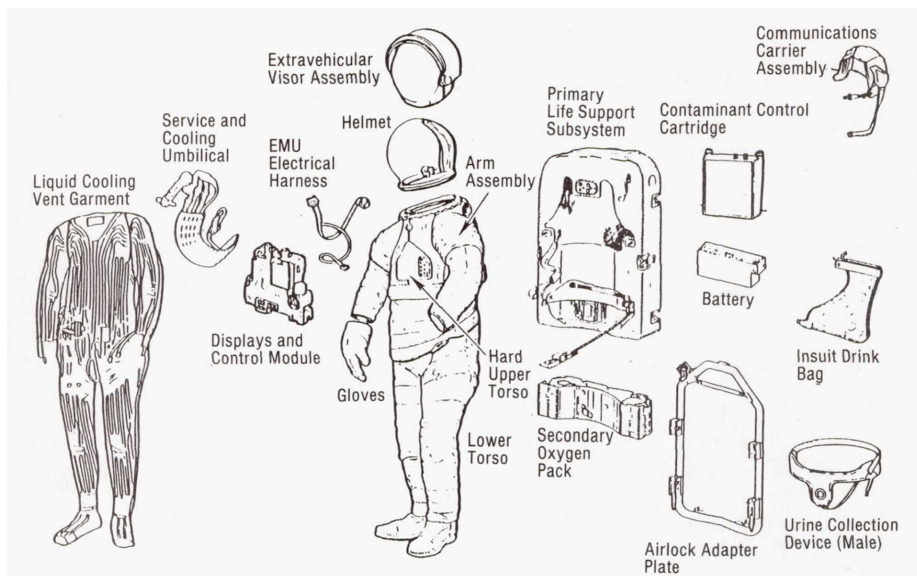


Figure 2-2: Components of Shuttle EMU. Image credit: (McMann & McBarron, 1985).

Figure 2-3 depicts each of the 14 layers of the EMU, which include cooling garments, pressure bladder and restraint layers, and micrometeoroid protection layers.

The EMU successfully kept astronauts safe and enabled EVA during the Shuttle and ISS era, but were not designed to be long-lasting (NASA, 2017). Additionally, astronauts incurred many health risks imposed by the EMU, including decompression sickness, thermal regulation, shoulder and hand injury, and inadequate nutrition and

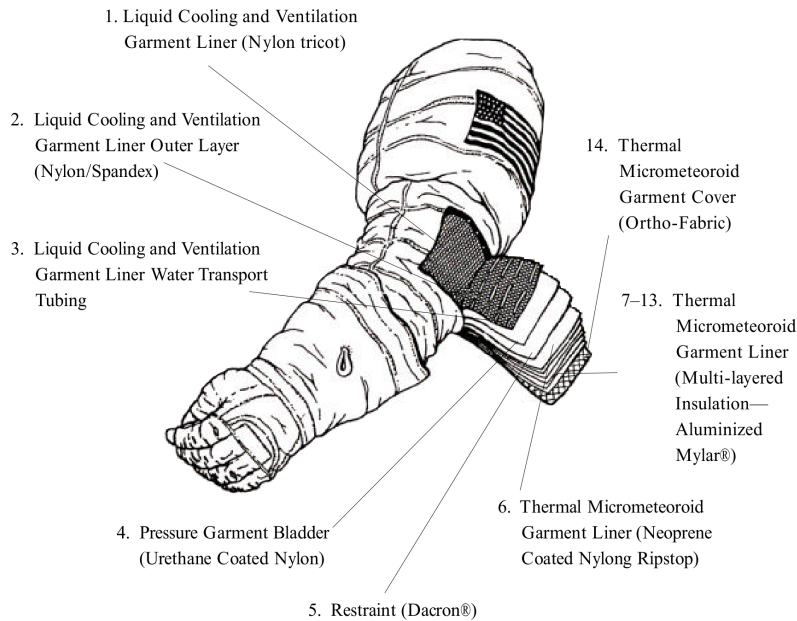


Figure 2-3: Layers of EMU. Image credit: (NASA, n.d.).

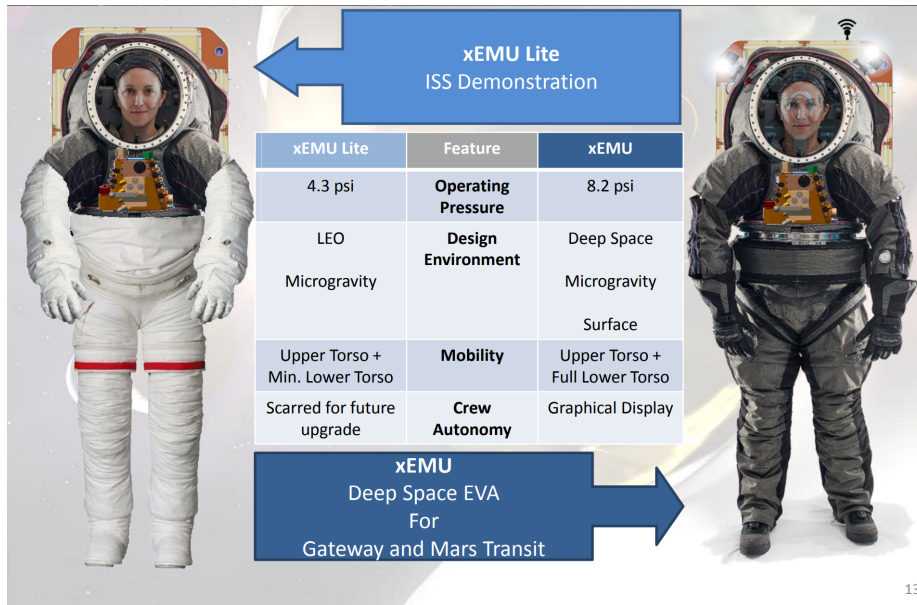
hydration (NASA, 2017). These health risks will be explored further in section 2.1.2.

With sights set on leaving low earth orbit (LEO) and returning to planetary bodies, the NASA Z-series space suits were conceptualized, with the Z-1 being completed in 2012 and Z-2 in 2015 (McFarland, 2016). The Z-2, shown in Figure 2-4A, is a rear-entry suit with updated hard upper torso durability, shoulder and hip joint mobility, and boots for traversing rough terrain (Roberts, 2015).

In 2019, NASA announced its astronauts will don the Exploration Extravehicular Mobility Unit (xEMU) for EVA on the upcoming Artemis missions. In recent years, there were several preliminary prototype xEMU demonstrations in preparation for the final xEMU design, such as the xEMU demo and xEMU Lite (see Figure 2-4).

The ground prototype of the xEMU that is planned for the upcoming Artemis missions is shown in Figure 2-5B.

Though NASA has not yet released many technical details regarding the xEMU, to date, gas-pressurized space suit designs have aimed to provide astronauts with the maximum range of motion while minimizing joint torque. However, current suits have limited joint range of motion and stiff joints, including knees, elbows, and shoulders,



13

Figure 2-4: Comparison of features between the xEMU Lite and xEMU intended for future planetary missions. Image credit: (Rodriggs, 2017).

A) Z-2 Prototype

B) xEMU Prototype



Figure 2-5: A) NASA Z-2 prototype. Image credit: (McFarland, 2016). B) NASA xEMU ground prototype. Image credit: NASA.

which impedes performance. Future designs should consider that some degree of knee joint torque could be beneficial in storing elastic energy during locomotion in partial gravity planetary EVA.

2.1.2 Astronaut Physiology and Performance in Reduced Gravity

Traditional gas-pressurized space suit designs, such as the EMU, aim to provide astronauts with the widest possible range of joint motion while minimizing joint torque during extra-vehicular activity. However, the many suit layers outlined in Figure 2-3, in addition to the stiff, pressurized limbs, result in significant joint torques exerted onto astronauts. Space suit joint torques exerted at the knee, as well as elbows, shoulders, hands, etc., can result in reduced astronaut range of motion and an increased risk of injury.

Range of Motion Impairment and Injury Risk

Astronauts wearing gas-pressurized space suits experience limited range of motion and stiffness at joints in the hands (Opperman, Waldie, Natapoff, Newman, & Jones, 2010), shoulder (Bertrand, Reyes, & Newman, 2016), (Strauss, Krog, & Feiveson, 2005), elbows (Diaz et al., 2012), knees (Gernhardt et al., 2009), and other joints. Norcross et al. (2010) related internal suit pressure with a user's mobility and task completion (Norcross & Clowers, 2010); therefore, suit design can lead to an impediment in EVA performance.

Additionally, the limited sizes available in the Hard Upper Torso can result in a decreased range of motion and an increased risk of shoulder injury (NASA, 2017), (Reid et al., 2014), (Williams & Johnson, 2019). Injury risk and discomfort could be further exacerbated by discrepancies between the anthropometrics of the wearer and the convolute joint alignment of the suit (Benson & Rajulu, 2009), (Strauss, 2004). Prior work has investigated the mechanisms that cause space suit injury, both during training and in-flight (Diaz et al., 2012), (Anderson, 2014), (Strauss et al., 2005).

The placement of suit bearings and the subsequent forced angles of rotation of limbs result in extremely limited movement capabilities (Anderson, Newman, & Welsch, 2015). Threats to mission success can arise from inefficient EVA due to decreased astronaut range of motion and increased injury risk in the EMU (Diaz et al., 2012). Work has also been performed analyzing how the biomechanical interaction between the astronaut and space suit impacts the fatigue and discomfort that astronauts experience (Anderson, Hilbert, Bertrand, McFarland, & Newman, 2014).

In light of the approaching missions to the Moon and Mars, there is an increasing importance for efficient EVA task performance in partial gravity. NASA has reported that the current EMU design, which is intended for use in microgravity, has nearly no mobility capabilities in the lower extremities (NASA, 2017). Though more recent space suits, such as the Mark III, have been developed to further planetary exploration capabilities, excessive joint torques in the hip lead to impeded mobility and agility of astronauts during locomotion (Cullinane, Rhodes, & Stirling, 2017), and mobility in knee flexion is still hindered (Norcross et al., 2009).

EMU Joint Torque

The joint torques exerted onto astronauts that result from stiff, pressurized space suit limbs have been characterized in different manners; calculating torques to bend an empty suit is one such method (P. B. Schmidt, 2011). These measurements have been collected for the EMU and Orlan suits (P. B. Schmidt, 2011), (Abramov, Stoklitsky, Barer, & Filipenkov, 1994). Schmidt used a robot to bend space suit joints and recorded the relationship between the torque exerted and resulting joint angle (P. B. Schmidt, 2011). Dionne also published the torques associated with bending space suits for various joints (Dionne, 1991). This thesis is specifically focused on the joint toques associated with the knee; Figure 2-6 shows example knee joint torque data gathered from (P. Schmidt et al., 2001).

Another method to characterize joint stiffness in space suits involves comparing human strength of a specific joint with the space suit donned and doffed. Morgan et al. used a joint dynamometer system to measure isolated joint strength (Morgan,

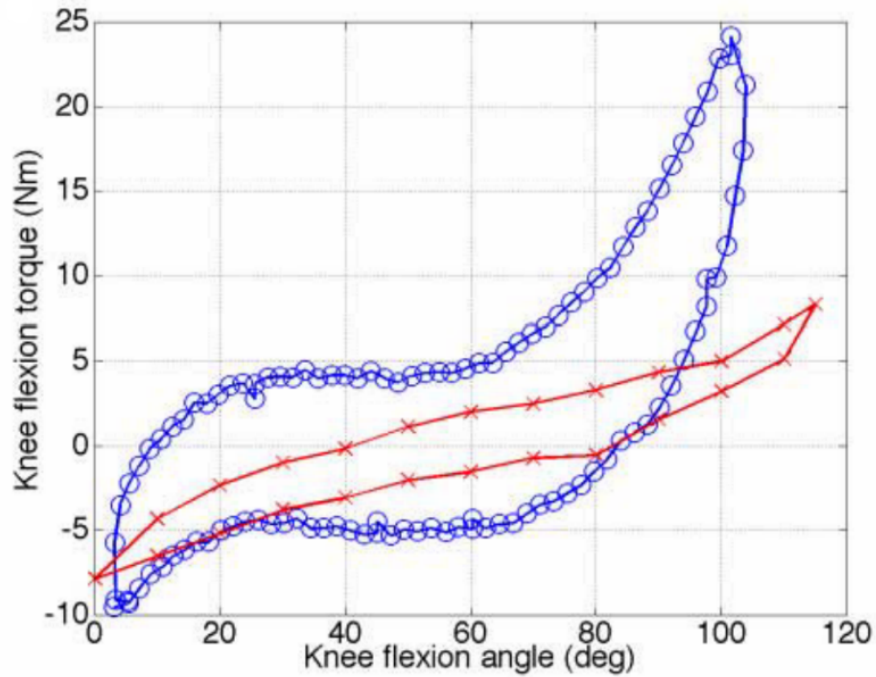


Figure 2-6: A) Knee joint EMU torques across a spectrum of flexion angles, measured in an empty suit joint. Data collected by Schmidt (blue) and Dionne (red) (P. Schmidt et al., 2001), (Dionne, 1991). Image credit: (P. Schmidt et al., 2001).

Wilmington, Maida, & Demel, 1996). The knee flexion/extension measurements were taken at a prescribed angular velocity of 60 deg/s. The measured torque to hold a knee joint at 72 degrees (where a 90-degree angle between the calf and shank was defined as a zero-degree neutral position) has been measured at 3.2 Nm (Dionne, 1991) and 6 Nm (Abramov et al., 1994) in empty suited conditions. Torques of 8.1 Nm (Morgan et al., 1996) and 3.74 ± 0.676 Nm (P. B. Schmidt, 2011) were measured in suited human conditions.

2.2 Mechanical Counterpressure (MCP)

Current EMU space suits in use on the ISS have enabled astronauts to successfully perform EVAs in a microgravity environment. These suits are pressurized to approximately 1/3 of an atmosphere, making it extremely fatiguing to fight against this suit a multi-hour EVA. This fatigue has been shown to lead to reduced mobility and joint

injury.

Astronaut fatigue in a space suit can be described by the work associated with deforming a pressurized garment; minimizing this deformation work would result in reducing overall fatigue. Innovative space suit development has included the possibility of mechanical counterpressure (MCP) and is being investigated as an alternative to gas-pressurization.

2.2.1 MCP vs. Gas-Pressure Suits

The prototype soft knee exoskeleton was developed to be integrated into an MCP space suit concept developed by Prof. Dava J. Newman at MIT. In order to define criteria for the soft knee exoskeleton, the importance of MCP must be established.

Metabolic cost during EVA depends on the work required to deform a space suit, which can be described in the following equation (Carr & Newman, 2007):

$$\Delta W = \Delta W_p + \Delta W_b + \Delta W_s \quad (2.1)$$

Where ΔW is total work, ΔW_p is pressure-volume work, ΔW_b is work to bend a space suit, and ΔW_s is work to stretch a space suit. Efficiency of work can be computed by the rate of change of work divided by the rate of change of metabolic expenditure.

Compared to the current gas-pressure space suit, MCP suits are theorized to decrease metabolic cost of locomotion in space suits by eliminating the work needed to deform the pressure-volume (ΔW_p in equation 2.1) (Obropta & Newman, 2015). Also, the increased range of motion of MCP suits relative to gas-pressurized suits would be beneficial in reducing the incidence of space suit-related injury reported by astronauts and increasing performance.

2.2.2 Space Activity Suit

MCP suits were initially explored by Webb and Annis in 1971 to mitigate vacuum effects in space by using seven layers of compressive materials to provide surface pressure to the user, rather than using gas to provide the equivalent pressure (Annis

& Webb, 2004). This suit was known as the Space Activity Suit (SAS) and is shown in Figure 2-7.

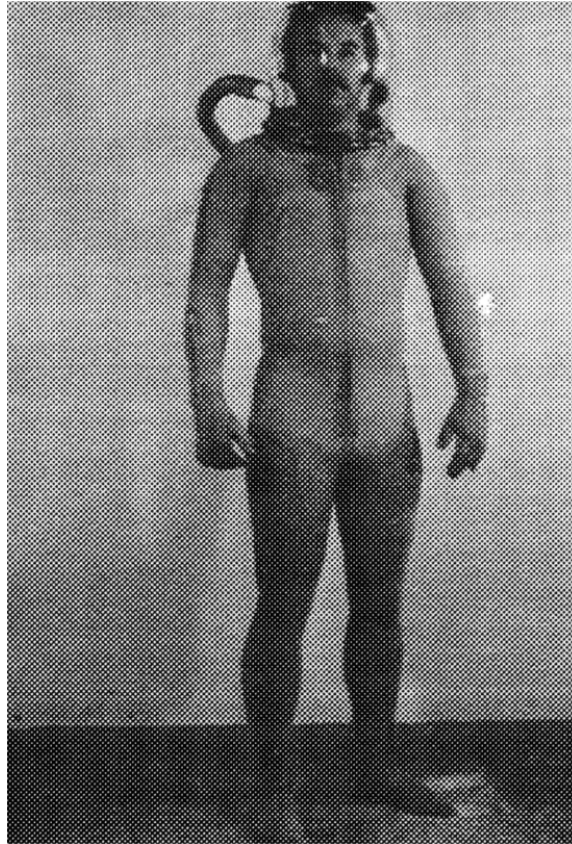


Figure 2-7: 1971 Space Activity Suit developed by Webb and Annis. Image credit: (Annis & Webb, 2004).

At the time, MCP suits were limited by insufficient material technology and issues in donning and doffing such tight garments (Obropta & Newman, 2015). However, the SAS was able to demonstrate the increased mobility benefits of MCP.

2.2.3 BioSuit™

The BioSuit™ is an example of an advanced MCP space suit concept, shown in Figure 2-8, and is being developed by the Human Systems Lab at MIT in collaboration with Dainese and the D-Air Lab (Vicenza, Italy) (Newman et al., 2005).

The BioSuit™ requirements include 5 mm thickness to act as a "second skin" and produce 29.6 kPa of pressure, which is equivalent to that produced by the NASA



Figure 2-8: Conceptual renderings of a conformal helmet and modular portable life support system for the BioSuit™ created by Michal Kracik (Kracik et al., 2012).

EMU (Holschuh, Obropta, Buechley, & Newman, 2012). Further details concerning the physiological significance of these criteria, including risk of edema associated with MCP, can be found in (Carr & Trevino, 2019).

Work has been done to develop a functional engineering prototype of the BioSuit™ (Figure 2-9) by evaluating materials that would apply uniform and consistent MCP at the required pressure.

Additionally, donning/doffing problems still exist (Anderson, 2011), (Judnick, Newman, & Hoffman, 2010). Active materials are being investigated as an option to constrict the suit around the body after it has been donned (Holschuh et al., 2012).

The BioSuit™ illustrates an example of a soft exoskeleton that aims to maximize locomotion mobility capabilities of an astronaut in order to conduct planetary exploration as efficiently as possible (Newman et al., 2005). By increasing dexterity and reducing the risk of injury to an astronaut, the BioSuit™ aims to compliment natural motion, thereby minimizing the metabolic workload required to traverse irregular terrain in an exploratory partial gravity environment, such as the Moon or Mars.



Figure 2-9: BioSuit™ illustrations and mock-ups with lines of non-extension patterning. Center image credit: Jeremy Stroming (Stroming, 2020). Left and right image credit: Dava Newman.

2.2.4 Lines of Non-Extension (LoNE)

If the BioSuit™ were to be augmented to provide tuned knee stiffness and aid in locomotion, it would be analogous to a lower body exoskeleton. However, soft exoskeletons are notoriously difficult to anchor actuation points to the compliant human body. Additionally, traditional exosuits do not deform similarly to the human. To overcome this issue, Lines of Non-Extension (LoNEs) are a vital aspect to MCP garments.

LoNEs were first measured by Iberall and evaluated in the context of an MCP suit in 1964 (Iberall, 1964). They were measured by analyzing the shape deformation of ink circles marked on the skin as a subject performed a variety of motions (Iberall, 1964). The circles deform into ellipses; these ellipses will have two diameters which do not change in the case of small skin strains, which can then be mapped over large surface areas of the skin (Iberall, 1964). Ink circle deformation and the sets of unchanging diameters of the resulting ellipses are shown in Figure 2-10.

Though Iberall was able to map LoNEs via this process of tracking inked circles,

the process was time consuming and prone to human-error. Bethke and Newman developed a method to digitally compute LoNEs via optical strain analysis and used this process to map leg LoNEs (Newman & Wessendorf, 2015) to be implemented into the BioSuitTM. To further this work, Wessendorf and Newman calculated LoNE around the knee using motion capture (Wessendorf & Newman, 2012). The processes of skin strain measurement used by Iberall, Bethke, Wessendorf, and Newman are consolidated into Figure 2-10. Obropta and Newman were able to calculate LoNE of the shoulder and elbow to sub-millimeter resolution using Digital Image Correlation (DIC) (Obropta & Newman, 2015), (Obropta & Newman, 2016).

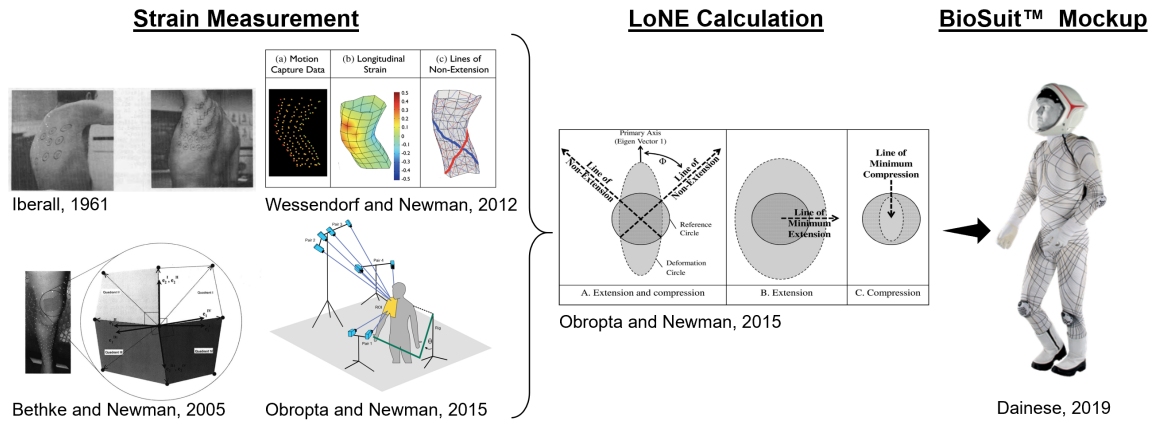


Figure 2-10: Strain measurement contributions from Iberall, Bethke, Wessendorf, and Newman to LoNE calculation for the mockup of the BioSuitTM. Adapted from (Iberall, 1964), (Newman & Wessendorf, 2015), (Wessendorf & Newman, 2012), (Obropta & Newman, 2015), and (Dainese, 2019).

Though these groups have calculated LoNE for various regions of the body, LoNE have not been precisely implemented into the current BioSuitTM mockup due to fabrication limitations.

LoNE integration into the BioSuitTM is necessary to maximize the efficiency of astronaut locomotion. This project aims to develop a tuned knee-joint capability could be beneficial in space suit energy conservation, though the direct integration of LoNE into the soft knee exoskeleton is outside the scope of this thesis. However, when designing the soft knee exoskeleton, it is vital to consider fabrication techniques that could be compatible with computed LoNEs for seamless integration into the BioSuitTM in the future.

2.3 Exoskeleton Mechanics

In order to accomplish the goal of designing a soft knee exoskeleton that provides a tunable stiffness to augment astronaut locomotion in reduced gravity, we must understand the biomechanics of human gait and energetics, as well as potential impacts that an exoskeleton may have on those mechanics and on metabolic cost. Prior work in soft lower body exoskeletons and the resulting metabolic impacts on the user should be reviewed to aid in design conceptualization. Finally, approaches to how computational modeling can be leveraged to inform exoskeleton design and characterization should be discussed in the context of human spaceflight.

2.3.1 Gait Overview

Human gait is composed of two events for each foot: heel contact and toe off, which occur across the stance and swing phases; these events are depicted in Figure 2-11. The stance phase consists of single support (one leg in contact with the ground) and double support phases (both legs are in contact with the ground). The time duration of one event to the next occurrence of that event is defined as one cycle of gait. For the purpose of this thesis, one cycle of gait is defined as the time between maximum knee extension.

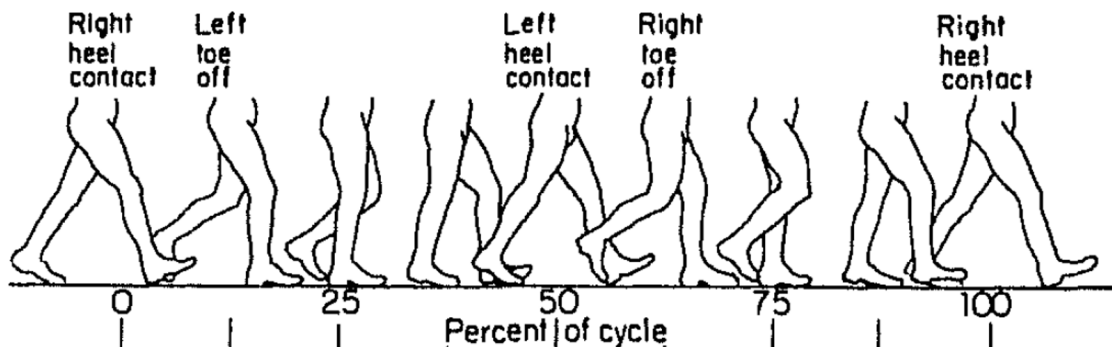


Figure 2-11: Phases of human gait cycle. Image credit: (McMahon, 1984).

The running cycle differs from walking by the presence of an increased velocity and an airborne phase where no leg is in contact with the ground (Dugan & Bhat,

2005).

Body center of mass motion has been studied to calculate potential and kinetic energy transfer during walking and running (McMahon, 1984). As gravity levels change, the potential energy storage of the body’s center of mass is altered. Therefore, locomotion in partial gravity differs than that on Earth; walking velocity limits are reduced due to decreased potential energy storage, consequently leading to diminished kinetic energy (McMahon, 1984). Rather than abiding by a slower walking speed, Apollo astronauts moved in a “loping” motion, which is defined by Rader, Newman, and Carr as “skipping without a foot exchange” (Rader, Newman, & Carr, 2007). Restrictive space suits may have also contributed to this gait adaptation (Rader et al., 2007).

Studying body kinematics and energetics during gait, such as joint angles, joint moment, ground reaction forces, and metabolic cost, are important metrics to evaluate the impact of a stimulus (such as an exoskeleton) on locomotion mechanics.

2.3.2 Exoskeleton and Space Suit Energetics

As mentioned in previous sections, pressurized space suits have stiff joints that can cause injury and increase the metabolic cost associated with locomotion when compared to walking unaided in 1G (Carr & Newman, 2007). However, these stiff joints may store elastic energy and positively impact locomotion in reduced gravity (Carr & Newman, 2017). Carr and Newman constructed a lower-body exoskeleton (Figure 2-12) with stiffness analogous to that of a space suit (Carr & Newman, 2008), and determined the presence of an unknown optimum stiffness at which metabolic cost is minimized, (see Figure 2-13, where $\frac{k}{k_{EMU}}$ is relative space suit stiffness) (Carr & Newman, 2017). Figure 2-13 represents two potential non-linear relationships between specific resistance and the relative leg stiffness measured in the study, ranging from completely unsuited to stiffness analogous to the EMU.

To elucidate where this optimum is, specific resistance of suited leg stiffness must be investigated across a spectrum of simulated gravity. Specific resistance, the energy expenditure to transport a unit mass over a unit distance, is calculated using the

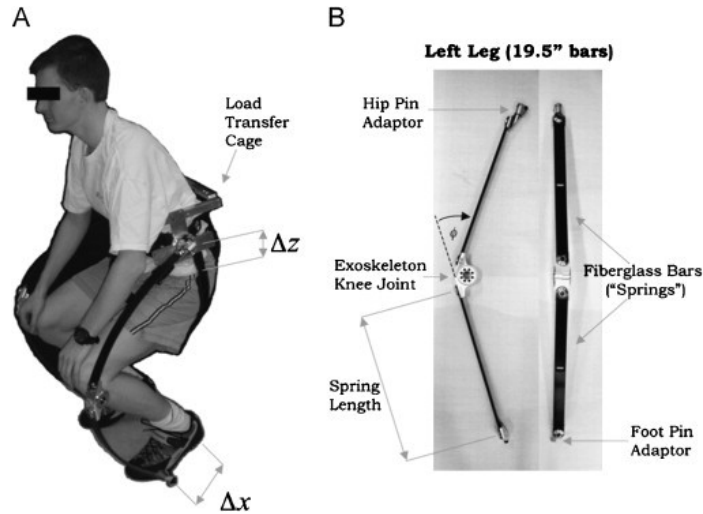


Figure 2-12: Exoskeleton (left) and fiberglass legs (right). Image credit: (Carr & Newman, 2008).

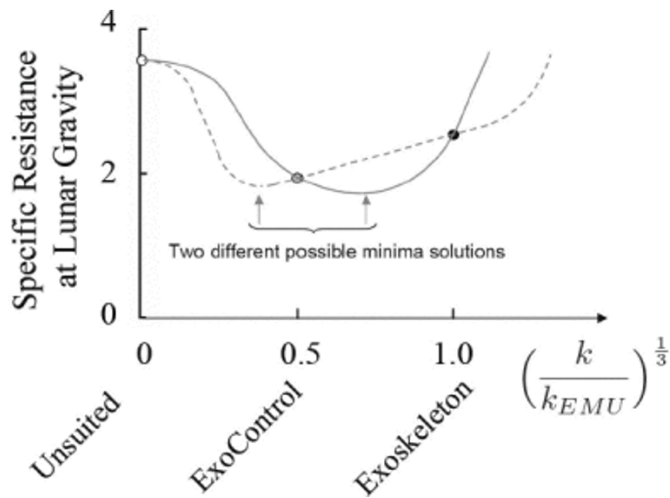


Figure 2-13: Proposed non-linear relationship between specific resistance with relative leg stiffness (where k represents stiffness). Image credit: (Carr & Newman, 2017).

following equation:

$$S = \frac{C_m}{-g} \left[\frac{J}{N \cdot m} \right] \quad (2.2)$$

Where C_m represents mass-specific transport cost (mass-specific metabolic rate/velocity) and S represents specific resistance (dimensionless) (Carr & Newman, 2017). A knee exoskeleton that is able to provide varying stiffness could be leveraged to perform this investigation across a gravity spectrum, including 1G, Lunar gravity (1/6 G) and Mars gravity (3/8 G). Such an exoskeleton could be integrated into the BioSuit™

design to provide optimum stiffness in each environment.

2.3.3 Tuned Knee Stiffness Biomechanics

The interaction between leg and surface stiffness is well understood and can approximated as a mass-spring model in which leg stiffness remains relatively unchanged (see Figure 2-14) in response to increases in velocity, but as the stiffness of the walking surface is altered, leg stiffness changes to accommodate this change (Blickhan, 1989), (McMahon & Cheng, 1990).

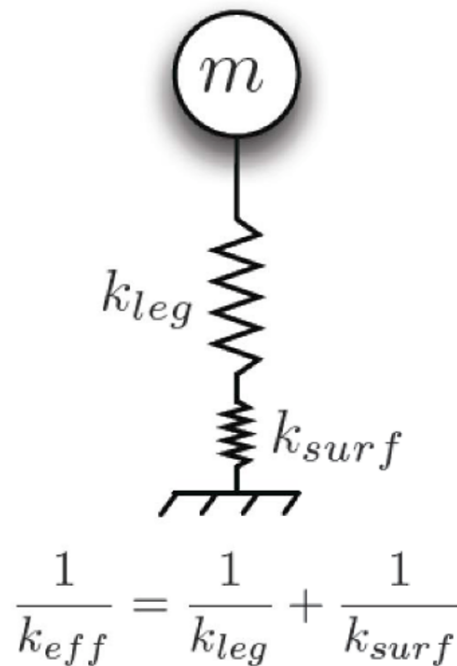


Figure 2-14: Spring-mass model of leg stiffness interaction with a surface. Image credit: (Carr & Newman, 2017).

McMahon investigated the effect of leg stiffness disruption on this model, and found that oxygen consumption increases significantly, potentially due to induced oscillations of the center of mass (Carr & Newman, 2017) Kerdok et al. found that effective leg stiffness (k_{eff}) does not change, despite changes in the surface, and instead leg stiffness increased in response a reduction in surface stiffness (Kerdok,

Biewener, McMahon, Weyand, & Herr, 2002). Since the leg and surface are in series in this model, the result of this compensatory leg stiffness modification is a similar effective leg stiffness (Carr & Newman, 2017). However, a reduction of as much as 12% is seen in metabolic cost with decreases in k_{surf} (Carr & Newman, 2017), (Kerdok et al., 2002). Since the k_{eff} was unchanged in these studies, it can be inferred that when the center of mass oscillations are constant and for each step, the muscles produce similar work. Furthermore, increased energy recovery with decreasing surface stiffness could be the source of the reduction in metabolic transport per step (Carr & Newman, 2017).

As Carr and Newman discuss in (Carr & Newman, 2017), though we know how the leg and surface stiffness interact, how springs in parallel with the human leg modulate leg stiffness remains unclear (Carr & Newman, 2017). To investigate this gap in knowledge, energy delivered by a surface can be calculated for the legs of the exoskeleton utilizing kinematic data. Carr postulates that in order to prevent changes in center of mass motion, k_{leg} would decrease with normal, 1G effective leg stiffness (Carr & Newman, 2017). Space suit knee joints may therefore have a large impact on leg stiffness in reduced gravity; this thesis seeks to help fill this gap in knowledge to establish a more comprehensive understanding of the regulation leg stiffness and use these data to drive the development of future space suits.

In summary: as outlined in section 2.3.2, Carr and Newman determined that there is some optimum stiffness of the knee exoskeleton at which metabolic cost is minimized during locomotion in reduced gravity, and this stiffness is likely lower than current EMU stiffness (Carr & Newman, 2017). A simple model for a knee joint that provides tuned stiffness is a spring and mass with space suit stiffness in parallel with the leg (Carr & Newman, 2017). Additionally, an ideal stiffness that minimizes metabolic cost would likely change in response to different gravitational levels (i.e., Earth (1G), Moon (1/6G), or Mars (3/8G)). Therefore, an exoskeleton that can provide a tuned level of stiffness exerted at a joint is desirable for a space suit that can operate across the gravity spectrum.

2.3.4 Lower-Body Soft Exoskeleton Actuation and Metabolic Cost Impacts

Exoskeletons for human performance augmentation are widely investigated in the field of engineering with applications including rehabilitation, load-carrying, and gait assistance to compensate for musculoskeletal inefficiencies. A majority of exoskeleton work has focused on rigid exoskeletons, which provide added bulk and inertia that can result in joints on the body not being aligned with joints of the exoskeleton, disrupting gait (Wehner et al., 2013).

Rigid exoskeletons often aim to accomplish these tasks by applying a torque at a particular joint or joints to help a user move more efficiently; historically, however, due to large mass and power requirements that accompany rigid exoskeletons, there is often a resulting increase in metabolic workload imparted on the user to operate the exoskeleton. In more recent years, exoskeletons have been developed specifically intended to reduce the metabolic cost associated with walking and running; a detailed review of these exoskeletons can be found here (Sawicki, Beck, Kang, & Young, 2020). Some of these exoskeletons leverage soft materials that provide a more comfortable interface with the human. These “soft exoskeletons” or “soft exosuits” use more lightweight materials and do not impose rigid joint limitations.

Various methods have been implemented in articulating soft exoskeleton joints. Dr. Conor Walsh and the Harvard Biodesign Lab have extensive experience in engineering soft exosuits. The Biodesign Lab has utilized McKibben-style pneumatic actuators (Wehner et al., 2013) (see Figure 2-15) and, more recently, Bowden cables have been used to route forces across joints (Asbeck, Schmidt, Galiana, Wagner, & Walsh, 2015), (Lee et al., 2018). An example of Bowden cable actuators in an exosuit can be found in Figure 2-16.

The pneumatic actuators in the soft lower-extremity exosuit in Figure 2-15 can actuate hip, knee, and ankle joints. In a pilot study, metabolic power was calculated for resting, unsuited, and suited at incremental powered ankle actuation for each subject and the corresponding hip, knee, and ankle kinematics were measured via



Figure 2-15: Soft exosuit utilizing pneumatic actuators. Image credit: (Wehner et al., 2013).

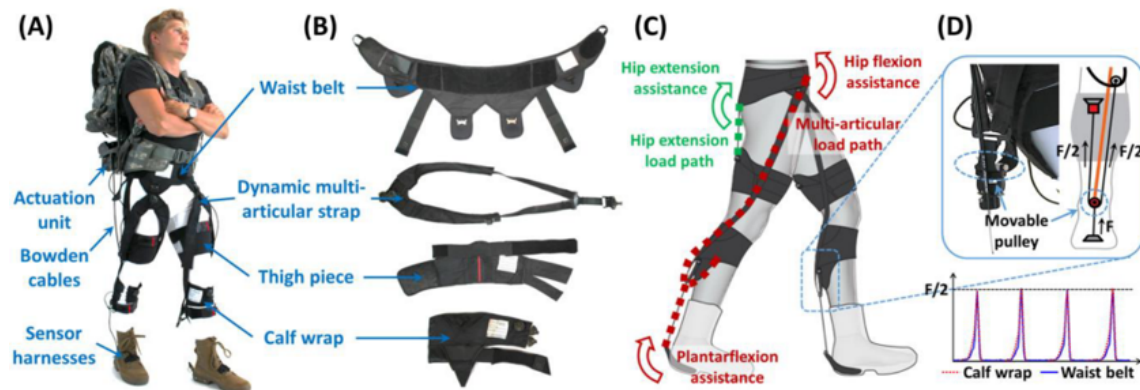


Figure 2-16: Soft exosuit utilizing Bowden cables. Image credit: (Lee et al., 2018).

VICON motion capture (Wehner et al., 2013). VO_2 and VCO_2 measurements were used to calculate metabolic power (Wehner et al., 2013). Actuation of the ankle joint does not have an apparent effect on the kinematics of the knee or hip sagittal plane angle (Wehner et al., 2013), suggesting that PAM actuation can provide isolated torques that do not impact the gait kinematics of the joint of interest, or of other major joints involved in gait. However, results showed that there was no metabolic cost savings associated with wearing the exosuit when compared to walking without the exosuit (Wehner et al., 2013).

Metabolic testing has also been conducted for a Bowden cable exosuit during plantar flexion actuation, which also transmits force for hip flexion assistance during

walking with the exosuit in powered off and powered on conditions with low, medium, high, and max levels of plantar-flexion actuation (Quinlivan et al., 2017). As the level of actuated assistance increased, the metabolic rate of walking was correspondingly decreased, resulting in a maximum $22.83 \pm 3.17\%$ decrease when compared to walking with the exosuit powered off (Quinlivan et al., 2017).

Soft exoskeletons have been shown as promising replacements for rigid exoskeletons and in successfully offsetting the metabolic workload required by a user during locomotion (Wehner et al., 2013), but little work has involved knee actuation. Further, there is a gap in soft exoskeleton research in the context of human spaceflight. Diaz-Artiles et al. are developing active soft robotic actuators to be incorporated into the EMU knee joint aid in partial gravity ambulation (Diaz-Artiles et al., 2020), but no soft exoskeletons have been developed for integration into an MCP advanced space suit concept, such as the BioSuitTM. As mentioned above, to study the knee stiffness of a space suit, Carr and Newman developed a passive lower-body exoskeleton to be analogous to the knee-joint torques of a pressurized space suit (Carr & Newman, 2008) and was found to aid in energy recovery and lower the metabolic cost of locomotion (Carr & Newman, 2007). An unknown optimum stiffness has been proposed, at which metabolic cost is minimized during locomotion (Carr & Newman, 2017). From this preliminary data and state of current soft exoskeleton technology, this thesis seeks to develop a passive soft knee exoskeleton that can apply adjustable stiffness to the knee while permitting full range of motion for flexion and extension to improve the metabolic efficiency of an astronaut during locomotion in partial gravity.

2.3.5 Musculoskeletal Modeling for Spaceflight

Current space suits clearly increase the risk of injury and limit the mobility of astronauts, which can directly lead to compromised EVA performance. Development of advanced space suits will require a comprehensive understanding of how suit torques are distributed throughout a body, body kinematics during EVA tasks, and quantitative characterization of metabolic cost to accomplish anticipated tasks to maximize EVA planning efficiency. Unfortunately, kinematic and kinetic data on the ISS ex-

ists in the context of exercise only. Further, the ISS is a microgravity environment, and due to the nearly 50-year hiatus since humans walked on the moon, kinematic partial gravity EVA ambulation data are strictly limited to video footage of Apollo astronauts traversing the lunar terrain.

Ground analogs, such as body weight offload systems and parabolic flights, are helpful surrogates to better understand human motion in reduced gravity in the absence of spaceflight data. However, these analog experiments can be costly and time-consuming. Computational models are a useful tool to generate a wealth of data for a fraction of the time and cost of live experiments. Such models would be valuable in performing simulations to inform space suit design, EVA route planning, and injury prediction.

Computational models have been developed that seek to assess injury risk by predicting human-space suit interaction, including rigid-body models that calculate forces exerted on the human by the suit (Schaffner, Newman, & Robinson, 2000), (Newman, Schmidt, & Rahn, 2000), (P. Schmidt et al., 2001), (H. Li, Jin, & Wang, 2012), (Diaz & Newman, 2014), (J. Li, Ye, Ding, & Liao, 2017). Stirling, Arezes, and Anderson summarize these space suit interaction models in the context of suit mobility evaluation and injury prevention (Stirling, Arezes, & Anderson, 2019).

These human-suit interaction models can be useful to help decrease straining and loading of tendons and muscles, as well as predict high-pressure points for a user performing an EVA in microgravity (Stirling et al., 2019); however, there is limited knowledge surrounding the effects of space suits on gait mechanics in partial gravity. Particularly, models exist that simulate the human-exoskeleton system for the lower body; some examples of these include exoskeletons of the full lower-body (Ferrati, Bortoletto, & Pagello., 2013), (Zhu, Zhang, Zhang, Liu, & Zhao, 2015), (Aftab & Ali, 2017); lower back (Manns, Sreenivassa, Millard, & Mombaur, 2017); ankle (Jackson, Dembia, Delp, & Collins, 2017), (Sawicki & Khan, 2016); and knee (Karavas, Tsagarakis, & Caldwell, 2012). However, there are extremely limited efforts to model these exoskeleton mechanics in partial gravity environments, which limits our ability to understand EVA locomotion mechanics.

OpenSim is an open source rigid-body musculoskeletal modeling software developed by Stanford University (Leth et al., 2018). This tool enables dynamic simulation of movement and provides a platform to investigate kinematics, kinetics, and muscle and muscle group activity. Modeling with OpenSim has been used in the context of rehabilitation, orthopedics, robotics, ergonomics, performance, and design. OpenSim can be leveraged to model a soft knee exoskeleton and perform metabolic analysis from the imposed joint loading to simulate locomotion in a partial gravity EVA. Kluis et al. have recently investigated OpenSim as a tool to model active robotic actuation at the knee of the EMU to assist ambulation; to date, these modeling efforts have been limited to 1G (Kluis et al., 2020). This thesis aims to similarly apply OpenSim to evaluate passive knee stiffness impacts on metabolic cost in both 1G and 0.17G.

2.3.6 Summary of Literature

In this chapter, we walked through the historical evolution of gas-pressure space suits, from the 1965 Berkut suit to the imminent xEMU. Range of motion impairment, injury risk, and knee joint torque associated with gas-pressure suits was highlighted. Mechanical counterpressure and advanced space suits (e.g. the BioSuitTM) were introduced. Exoskeleton mechanics, including gait overview and exoskeleton space suit energetics, were outlined to provide a foundation understanding of the benefits of tuned knee stiffness in EVA. Finally, the metabolic impacts of lower-body soft exoskeletons and potential methods to model such impacts via musculoskeletal modeling were described.

Chapter 3

Methods and Prototyping

This chapter describes the methodology of soft knee exoskeleton construction and evaluation via musculoskeletal modeling. Design criteria were established to guide the production of the soft knee exoskeleton. Fabrication techniques, including Whole-Garment knitting and Computer Aided Design (CAD), were utilized to produce each prototype (Porter et al., 2020). Preliminary data are reported that characterize the stiffness of the soft knee exoskeleton. OpenSim gait modeling was leveraged to computationally evaluate the impact of applied knee stiffness on gait energetics for 1G and Lunar gravity (0.17G) testing conditions.

3.1 Soft Knee Exoskeleton Design Criteria

This section establishes relevant criteria that the soft knee exoskeleton should satisfy. As discussed earlier, Carr and Newman determined that there is some optimum stiffness of the knee exoskeleton at which metabolic cost is minimized during locomotion in reduced gravity, and this stiffness is likely lower than current EMU stiffness (Carr & Newman, 2017). Additionally, an ideal stiffness that minimizes metabolic cost would likely change in response to different gravitational levels (i.e., Earth (1G), Moon (0.17G), or Mars (0.38G)). Therefore, an exoskeleton that can vary the level of stiffness exerted at a joint is desirable for a space suit that can operate across the gravity spectrum.

Carr and Newman defined three design criteria:

1. The soft knee exoskeleton method of articulation shall provide stiffness in parallel with the knee.
2. The soft knee exoskeleton method of articulation shall provide rotational stiffness to hinder knee flexion.
3. The soft knee exoskeleton shall provide adjustable levels of stiffness.

The long-term goal of this work is to integrate the soft knee exoskeleton tuned stiffness capability into the BiosuitTM. Therefore, the actuation of this stiffness must not inadvertently reduce the mechanical counterpressure that the BioSuitTM requires. Furthermore, the method of articulation should not create a significant draw on the space suit power supply. From these needs two additional design criteria are added:

1. The soft knee exoskeleton stiffness actuation shall minimize power drawn from suit reserves.
2. The soft knee exoskeleton shall not diminish the MCP provided by the BioSuit.

3.2 Fabrication Techniques

The second aim of this design paper is to explore fabrication techniques to develop a soft knee exoskeleton. This section outlines the iterative process used to manufacture various prototypes.

3.2.1 WholeGarment Knitting

WholeGarment knitting utilizes computer-aided design to produce apparel that is knitted in three-dimensionally, rather than by knitting several pieces and sewing them together. WholeGarment knitting also enables the designer to experiment with different fiber types to achieve desired material behaviors. A prototype was developed to demonstrate a proof-of-concept method of production for a wearable sleeve that could

provide compression to aid in exerting sufficient MCP via WholeGarment knitting. This sleeve fabric would be used as the soft exoskeleton base fabric. Here, base fabric refers to the fabric surrounding the actuators, which would aid in producing MCP. Hoop strain theory was leveraged under the assumption that pressure is exerted on a thin-walled vessel and that the fabric is perfectly elastic; the calculation of hoop strain can be derived by the following relationship (Obropta, 2015):

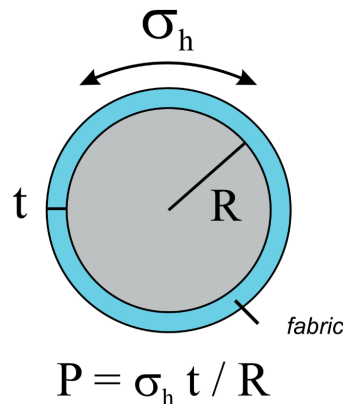


Figure 3-1: MCP calculation where P is pressure, R is limb radius, t is fabric thickness, and σ_h is hoop stress exerted by fabric (Obropta, 2015)

Three initial MCP sleeve prototypes, shown in Figure 3-2, were fabricated using Shima Seiki WholeGarment knitting. These sleeves were constructed with three different initial diameters, lengths, and widths of cuffing on the distal end of the sleeve.

These prototypes successfully demonstrated our ability to produce customized sleeves using WholeGarment knitting, which is vital to produce a base fabric for the knee exoskeleton, which is customized to fit the user. However, upon donning the sleeves, it was apparent that they exerted a compressive pressure much lower than the MCP goal of 29.6 kPa. Though the overall compressive capacity of the sleeves were insufficient for the BioSuitTM, the knit still resulted in difficulty donning the sleeves because of the low elasticity of the cuffs. The cuffs were therefore eliminated in future designs. Additionally, the final knee exoskeleton requires fibers of varying elasticity and stiffness. A second iteration of 3D sleeves was knitted, shown in Figure 3-3. Figure 3-4 depicts each sleeve on a mannequin arm.



Figure 3-2: First iteration of WholeGarment-knitted sleeves



Figure 3-3: Second iteration of WholeGarment knitted sleeves.

A final prototype was knitted with stiffer yarns used in conjunction with high-elasticity yarn in order to apply a more compressive force, shown in Figure 3-5.

Leferon polyamide yarn ($PA678/24/2$) in combination with synthetic elastomeric (Spandex) yarn were chosen for the final fabric prototype material in Figure 3-5. The synthetic elastomeric yarn increased the compression of the garment and the polyamide yarn provided elasticity. Further details on the material properties of these yarns can be found in Appendix A, Table A.1 and Table A.2. Tubular shaping with 1x2 rib stitching was used; rib stitching enables inlay of the synthetic elastomeric



Figure 3-4: Second iteration of WholeGarment knitted sleeves placed on mannequin arms.



Figure 3-5: Final base fabric prototype (left) placed on a mannequin arm (right).

yarn. Additionally, rib stitching provides increased elasticity of the material when compared to other stitching types (i.e., stocking stitch). The stitching and shaping techniques leveraged in the final base fabric iteration (Figure 3-5) were chosen to guide the design of the base fabric for the knee exoskeleton. However, the Spandex in the final base fabric prototype could not be implemented into the knee sleeve material,

which is explained in further detail below.

3.2.2 Airbag Fabrication

NASA reports that the torques exerted by space suits on the user are approximately -40 Nm for knee flexion to 11.3 Nm for knee extension (Meyen, 2013). Meyen analyzed several models of space suits and defined the minimum/maximum knee torque as -40 and 32 Nm, respectively, along with the angle of knee flexion and extension. For this exoskeleton, actuators that could resist flexion were sought (Figure 3-6). Pneumatic actuators, such as pneumatic artificial muscles, have been demonstrated as flexion and extension actuators in other soft exoskeleton projects (Wehner et al., 2013). The D-Air Lab (Vicenza, Italy) specializes in human protection through airbag and innovative technologies. The MIT Human Systems Laboratory partnered with the D-Air Lab to manufacture a soft knee exoskeleton with integrated airbags that provide stiffness in parallel with the knee by inhibiting flexion. Once airbags near the skin are inflated, they exert added mechanical counterpressure onto the tissue, thereby providing an additional advantage of utilizing airbag actuators. Based on these benefits associated with airbags, they were chosen as our stiffness actuators.

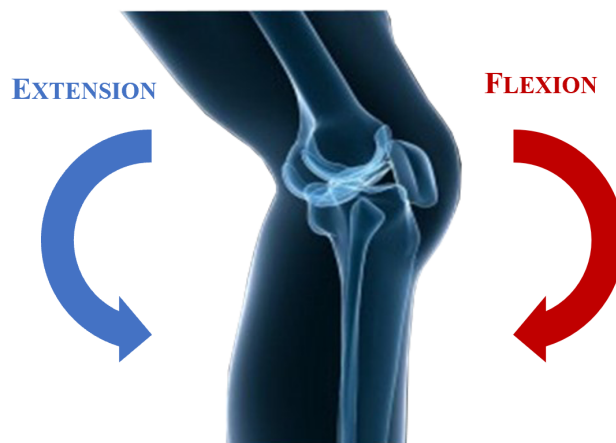


Figure 3-6: Knee joint rotation during flexion and extension (image adapted from (NASM, 2015)).

Figure 3-7 depicts the conceptual design of the air bag configuration that would provide this stiffness in parallel with the knee; the airbags were arranged with vertical

beams on the lateral and medial side of the knee, acting as a torsional spring to resist flexion. Additionally, horizontal airbags were designed to wrap from the posterior surface of the thigh and calf around the anterior surfaces to serve as anchor points and apply counterforces to aid in resisting knee flexion.



Figure 3-7: Conceptual airbag (green) configuration design (image adapted from (NASM, 2015)).

Since the final goal of the knee soft exoskeleton includes implantation into the BioSuit™, a method of fabrication was needed that could be leveraged to provide MCP. To begin this process, the D-Air lab inflatable airbag technology process was applied to exert flexion-inhibiting stiffness on the knee. The D-Air Lab fabricates airbags by first using WholeGarment knitting to create an enclosed knitted shape that accounts for the desired contours of the airbag garment or personal protection device (i.e., motorcycle suit) (Ronco, 2014). Then a polyurethane adhesive layer is affixed to the inflatable airbag, which enables the bag to become air-tight and maintain its ability to be re-inflated over time (Ronco, 2014).

Previously, airbags were fabricated separately from the garment and inserted into a pocket placed in the garment. However, for the exoskeleton MCP sleeve, the fabric of the sleeve must deform as similarly to the skin as possible to enable full range of motion, and a pocket embedded in the sleeve would be bulky and difficult to deform. Therefore, a process was developed to integrate the inflatable airbag directly

with the knee sleeve fabric, shown in Figure 3-8. WholeGarment knitting produces three-dimensionally knitted apparel and provides the capability of designing a custom airbag with dimensions fitted to a particular wearer, and additionally provides greater freedom in selection of yarns and fibers to fuse the airbag to the knee garment. This knitting method also affords the capability of designing embedded pockets into base fabrics. This double layered embedded pocket is laminated with a polyurethane adhesive layer and secured with applied heat and pressure, which converts the double layered pocket into an airbag.

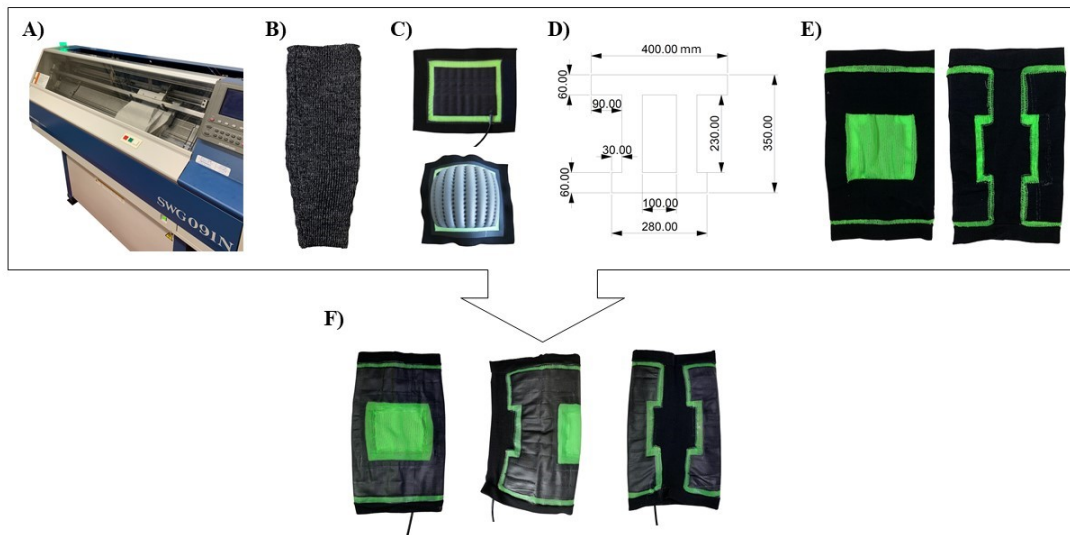


Figure 3-8: A) Shima Seiki SWG 091N machine was employed for WholeGarment knitting of integrated airbag and knee sleeve. B) Base fabric sleeve. C) Deflated (top) and inflated (bottom) example of airbag integrated into sleeve base material. D) CAD diagram of airbag orientation and measurements in mm. E) WholeGarment-knitted soft knee exoskeleton sleeve without lamination. F) Final soft knee exoskeleton with laminated airbags. (Porter et al., 2020).

CAD software was used to design the airbag configuration fitted to one user, from which the first iteration of the soft knee exoskeleton was knitted. The Shima Seiki machine uses yarn guides to lay each different spool of yarn into the needle bed, where the knitting occurs. While the soft knee exoskeleton is knitted by the Shima Seiki model SWG 091N, there are not enough yarn guides in this model to include the

Spandex fabric used in the final base fabric prototype, shown in Figure 3-5. Therefore, the soft knee exoskeleton contains only the Leferon polyamide yarn.

Knitting the soft knee exoskeleton required two separate yarn types to present different characteristics and functionality of the material. The external portion of the sleeve were made with the Leferon polyamide yarn (PA 6 78/24/2) used in the final base fabric prototype. An Expotex (Stezzano, Italy) thermoplastic polyurethane (TPU) yarn (CY 325-156 TPU/Nylon) was used for the airbag boarder and knee panel on the anterior face of the soft knee exoskeleton. The garment was knitted on a Shima Seiki G15 flat knitting machine with a tubular shaping technique. The base fabric knitting techniques described above were leveraged to surround the airbag and test its ability to maintain structural integrity of the seam between the airbag and the fabric over repeated airbag inflation. See Figure 3-9 for a diagram of this base fabric combination with the air bag. Cross stitching was implemented into the knitting of the airbag to prevent excessive ballooning, shown in Figure 3-9.

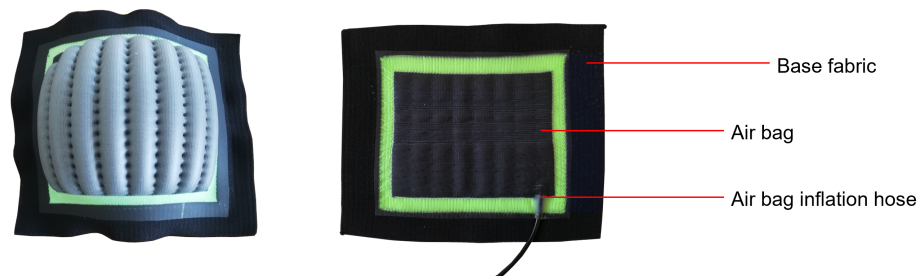


Figure 3-9: Base fabric and inflated airbag (left) and deflated airbag (right).

The CAD sketch of the first iteration of airbag design is shown in Figure 3-10, where all of the dimensions are in millimeters.

From the CAD sketch (Figure 3-10) and base fabric design, the Seimi Seiki machine was used to knit the first prototype soft knee exoskeleton, followed by lamination of the airbags. The anterior knee panel was knitted with a 2x1 rib stitch to maintain dimensional stability and enable increased elasticity in the knee to compensate for anticipated flexion. The remaining material was knitted with the 1x2 ribbing described above. The first iteration of this design is shown in Figure 3-11, henceforth referred to as soft knee exoskeleton Version 1 (V1). Unfortunately, the elastic base fabric

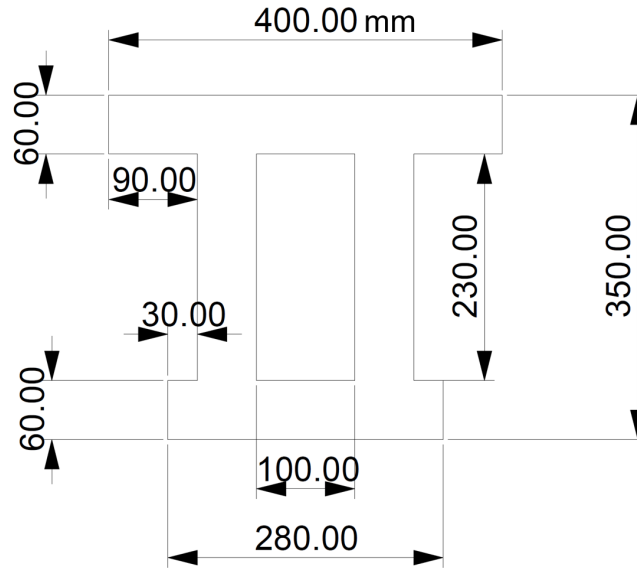


Figure 3-10: Sketch of knee airbag structure, dimensions in mm.

separating the airbags on the posterior side of the exoskeleton was too inelastic for ease of donning and doffing the exoskeleton. Additionally, there was an imperfection in the lamination that resulted in loss of pressure upon inflation.



Figure 3-11: Anterior (left), lateral (center), and posterior (right) views of soft knee exoskeleton V1 with insufficient elasticity of base fabric separating posterior airbags (circled).

A second iteration of the soft knee exoskeleton prototype was knitted with an

overall larger diameter. The elastic base fabric separating the airbags on the posterior side of the exoskeleton was widened for easier donning/doffing. The sleeve, henceforth referred to as soft knee exoskeleton Version 2 (V2) following airbag lamination is shown in Figure 3-12.



Figure 3-12: Soft knee exoskeleton V2 anterior (left) and posterior (right) views.

Upon donning V2, excessive gaping was noted behind the knee that resulted in a poor fit to the user. The horizontal air bag channels created a convolute joint that reduced the exerted stiffness qualitatively felt by the user. Convolute joints have historically been used in space suits to improve mobility at the joint. However, increased flexibility at the knee as a result of the convolute joint would directly negate from the desired exerted stiffness by the soft knee exoskeleton. Figure 3-13 illustrates these issues in V2 fit.

To alleviate these fit issues, soft knee exoskeleton prototype Version 3 (V3) was constructed. An AutoCAD drawing of V3 can be found in Appendix A, Figure A-1. Clo 3D Fashion Design Software (New York City, NY) was employed to generate a 3D CAD model with the desired design updates. Clo 3D is widely used for garment design and has some degree of inflation modeling capabilities. Design updates include:

- Circumference reduction in the distal cuff



Figure 3-13: Soft knee exoskeleton V2 donned (left) and maximally inflated (right). A) Anterior view. B) Lateral view.

- More dramatic sleeve tapering around the knee
- Increased overall sleeve length
- Change existing horizontal air bag channels to vertical to eliminate convolute joint

V3 with the aforementioned design updates is shown in Figure 3-14.



Figure 3-14: Soft knee exoskeleton V3 donned and maximally inflated anterior (left) and lateral (right) views.

Through Clo, a garment model of the soft knee exoskeleton was constructed. The sleeve was placed on a custom avatar whose leg reflects the anthropometric measurements of the anticipated subject pool for eventual human-in-the-loop experimental data collection. Clo includes a feature that allows the modeled airbags to be inflated, but only up to an internal pressure of 100 Pa. Strain plots can be created that illustrate the strain field of the garment when placed on the body. This feature was useful in the exoskeleton prototype design process, because it ensured that the measurements of the prototype were modified in a manner which resolves the fit issues in prototype V2. Inflating the airbags to the maximum pressure that Clo provides also helped to predict how the strain would change upon inflation; though 100 Pa is much lower than the anticipated maximum internal pressure of the physical prototype (which was anticipated to be nearly 100 kPa), the feature provided a conceptualization of strain changes upon inflation. It should be noted that the selection of garment materials is very limited in Clo, so the strain model does not consider the composition of the physical soft knee exoskeleton material. Each modeled strain field and corresponding rendering view is shown in Figures 3-15 and 3-16.

Deflated 3D Clo Model:

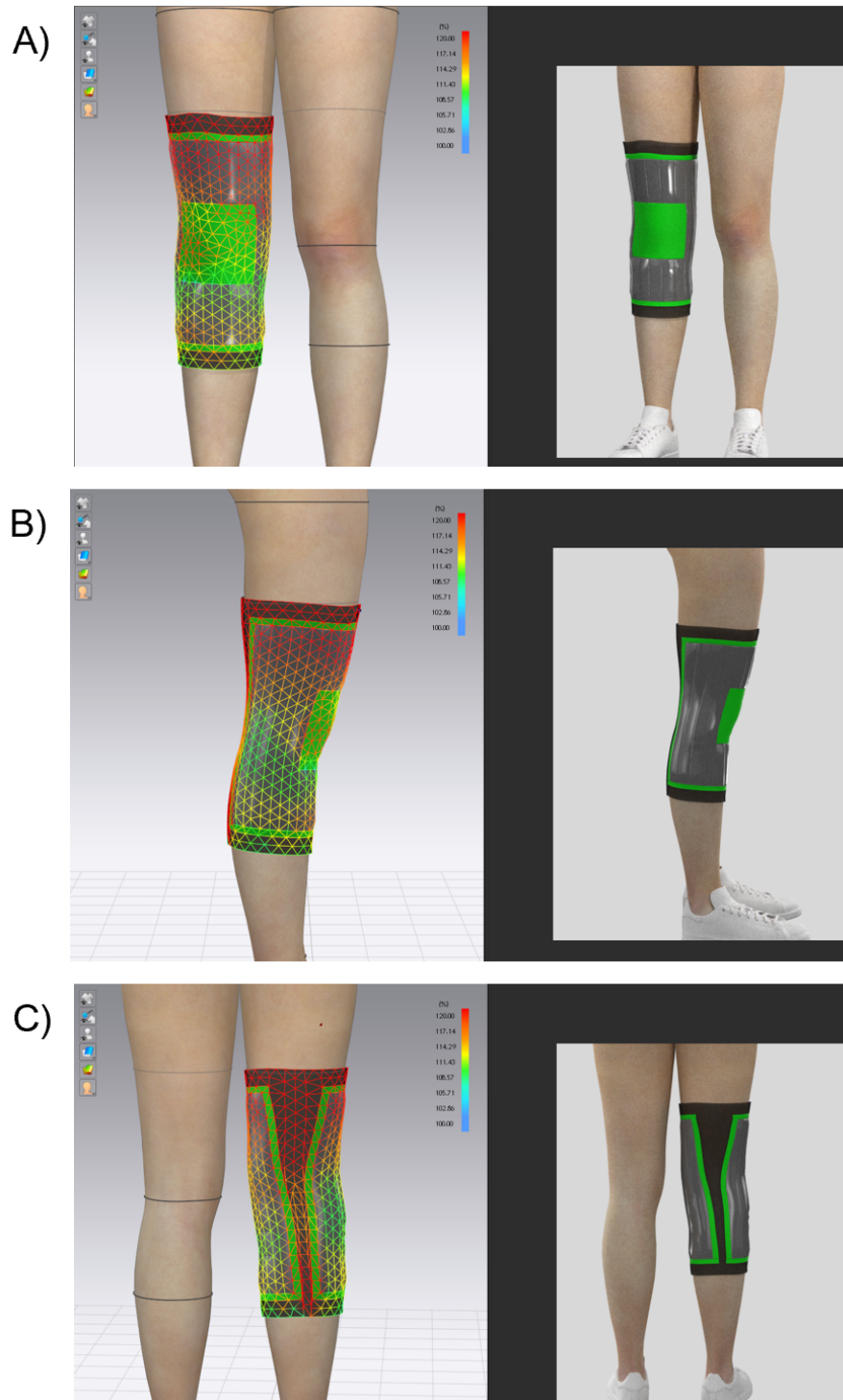


Figure 3-15: Model strain field (left) and rendering (right). Deflated A) Lateral view. B) Anterior view. C) posterior view. Green = lowest strain, red = highest strain.

Inflated 3D Clo Model:

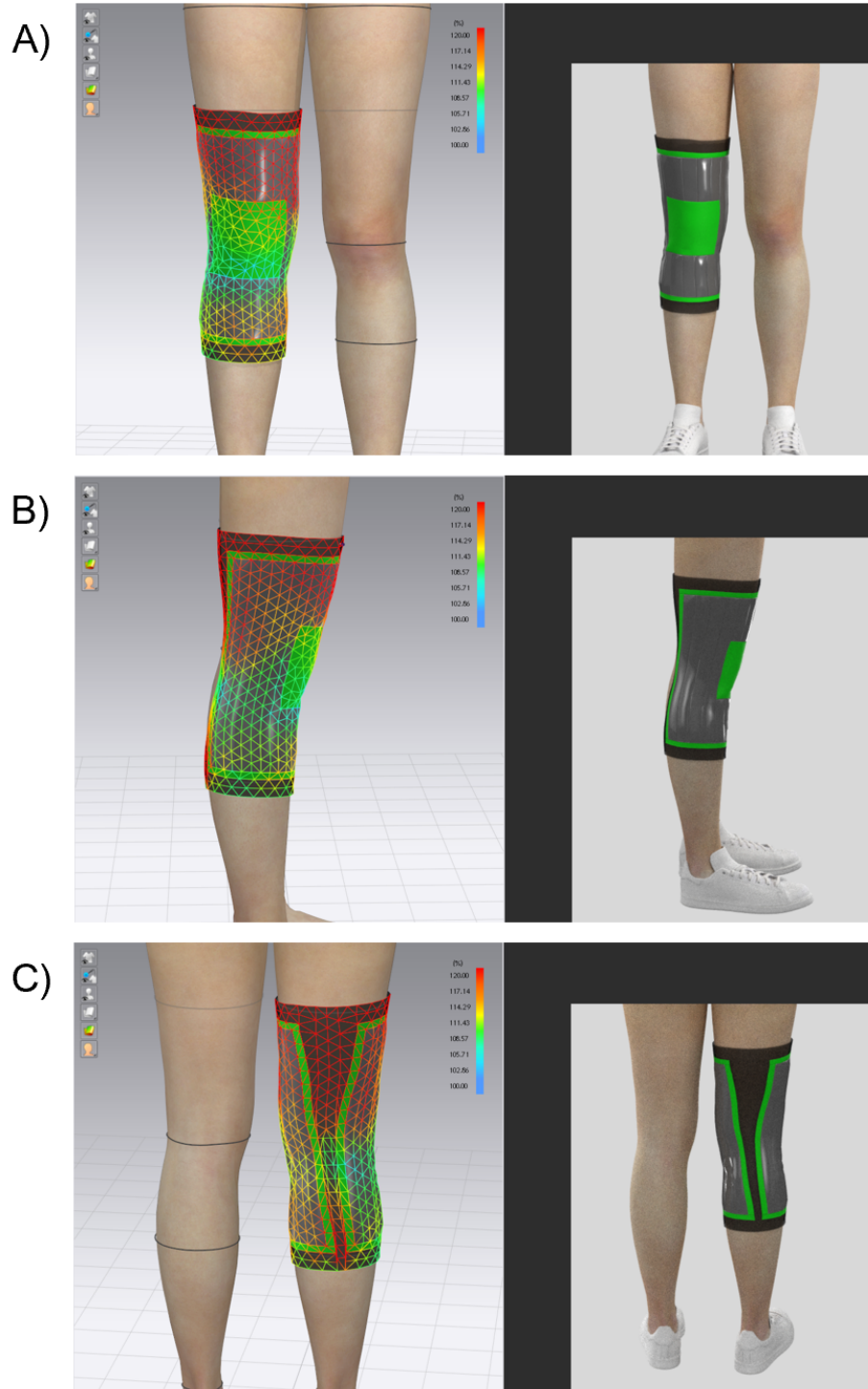























Figure 3-16: Model strain field (left) and rendering (right). Inflated A) Lateral view. B) Anterior view. C) posterior view. Green = lowest strain, red = highest strain.

For comparison, multiple views of prototypes V1, V2, and V3 are depicted in Table 1.

Table 3.1: Anterior, Lateral, and Posterior views of Prototypes V1, V2, and V3 in donned/doffed and inflated/deflated conditions.

Prototype Version	Condition	Anterior View	Lateral View	Posterior View
V1	Doffed, Deflated			
V2	Doffed, Deflated			
	Donned, Deflated			
	Donned, Inflated			
V3	Doffed, Deflated			
	Donned, Deflated			
	Donned, Inflated			

3.2.3 Preliminary Airbag Characterization

In order to characterize the stiffness exerted by the airbags in the soft knee exoskeleton, a test bench was configured through the University of Padova (Padova, Italy) and the D-Air Lab (Vicenza, Italy). A custom mechanical leg model with a knee hinge was fabricated to match the sizing of the prototype and enable measurement the stiffness of the leg sleeve in response to the leg model knee flexion. Load cells and angle sensors collect deflection and force measurements during model knee flexion and trigonometric relationships were used to calculate the exerted moment at the knee. The resulting linear model representing the stiffness of the soft knee exoskeleton and mechanical leg model system is depicted in Figure 3-17.

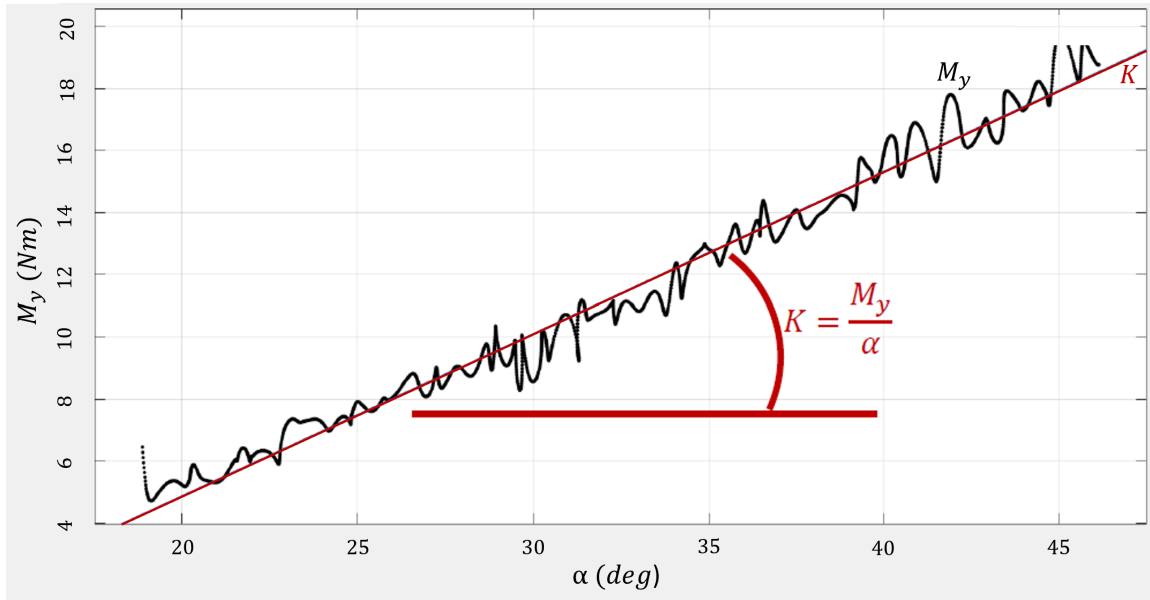


Figure 3-17: linear relationship between soft knee exoskeleton and mechanical leg model flexion angle (α) and moment (M_y). The slope represents system stiffness (K).

A reference value identified as the representing the stiffness from the mechanical leg model with the donned deflated sleeve. The inflated sleeve stiffness was then calculated from the difference between the reference value and the total stiffness of the leg model and inflated sleeve. A maximum moment value is collected at 45 degrees, listed in Table 3.2 for each pressure level of the inflated soft knee exoskeleton.

Table 3.2: Preliminary stiffness value and maximum torque at 45 degrees for each soft knee exoskeleton inflated pressure. Adapted from D-Air Lab measured results.

Nominal Pressure [kPa]	Preliminary Stiffness [Nm/deg]	Moment at 45 deg [Nm]
30	0.089	4.005
50	0.176	7.92
90	0.324	14.58

3.3 Modeling in OpenSim

The second Specific Aim of this thesis is to investigate the impact of varied stiffness prescription on locomotion mechanics and metabolic consumption in Earth and Lunar gravity using computational simulation of walking. The OpenSim2932 lower-body model and sample walking data were leveraged to generate a muscle-driven simulation with a knee spring with stiffness analogous to the soft knee exoskeleton. Joint kinematics, moments, estimated muscle metabolic cost during unassisted walking simulations in 1G were compared to soft knee exoskeleton assisted 1G walking simulations.

Though OpenSim sample gait data were provided for unassisted 1G walking, no sample data exists for partial gravity conditions. Partial gravity unsuited ambulation motion capture and ground reaction force data supplied by the NASA Johnson Space Center (JSC) Anthropometry & Biomechanics Facility (ABF) were implemented to tune the modeled knee exoskeleton to varying magnitudes of stiffness. Inverse kinematics and inverse dynamics were performed to compare estimated muscle metabolic cost during unassisted model walking simulations to the modeled soft knee exoskeleton conditions in partial gravity.

3.3.1 OpenSim Lower Body Extremity Model

OpenSim includes several generic models that specialize in various motions and muscle groups for users to choose from that meet their specific modeling needs. The Gait2392 model represents 76 lower extremity and torso muscles and 23 degrees of freedom (DOF) using 92 musculotendon actuators and was adopted from Delp et al. (Delp et al., 1990). A list of muscles present in the Gait2392 model can be found in Appendix

B, Table B.1. The default, unscaled version of this model represents a subject that is about 1.8 m tall and has a mass of 75.16 kg. Prior work has used these models to investigate joint moments, surgical effects on generating muscle moments, and muscle contributions and joint loading in response to motion (SimTK, 2020a). Recently, Diaz-Artiles et al. used an OpenSim gait model to evaluate robotic actuation in the EMU space suit during 1G ambulation (Diaz-Artiles et al., 2020), (Kluis et al., 2020).

The knee joint is composed of the femur, patella, and tibia. In addition, the lateral and medial collateral ligaments, lateral and medial menisci, and anterior and posterior cruciate ligaments provide stability and cushion to the joint. This multi-bone assembly combined with complicated ligament structure make the knee notoriously difficult to model. To alleviate these complications and ease computational complexity, the Delp et al. model uses an adapted single DOF model originally developed by Yamaguchi et al. to include sagittal plane kinematics for the tibiofemoral and patellafemoral joints and patellar levering (Yamaguchi & Zajac, 1989), (SimTK, 2020a). Delp et al. used the knee angle function to define femoral, tibial, and patellar reference frame transformations (SimTK, 2020a). Femoral condyles and tibial plateau are modeled as ellipses and a line segment, respectively (SimTK, 2020a). As the knee angle changes, the femoral condyles connect with the tibial plateau when the femoral reference frame is transformed to the tibial reference frame (SimTK, 2020a). The contact point between the tibia and femur is represented as a function of knee angle as described by Nisell et al. (Nisell, Nemeth, & Ohlsen, 1986), (SimTK, 2020a). Gait2392 does not include the patella, but instead models the quadriceps insertion point in the tibia as tibial frame moving points (SimTK, 2020a). These knee geometries are illustrated in Figure 3-18.

Provided with Gait2392 is an experimental data set that can be used to calculate musculoskeletal kinematics and dynamics. The experimental data set represents marker trajectories collected via motion capture (Vicon, Oxford, UK) collected at 120 Hz and center of mass motion calculated via ground reaction force plates (AMTI, Watertown, MA) collected at 1080 Hz (Schwartz, Rozumalski, & Trost, 2008).

OpenSim supports the capability to compute Inverse Kinematics (IK), Inverse Dy-

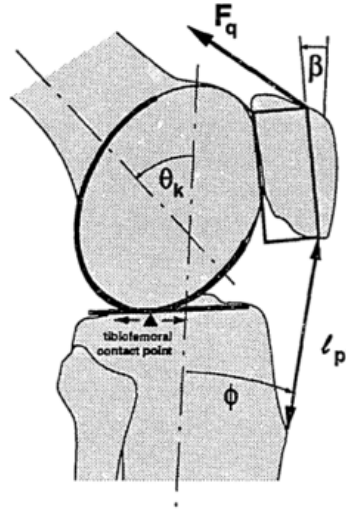


Figure 3-18: Delp et al. sagittal plane geometries. Image Credit: (Delp et al., 1990).

namics (ID), and Computed Muscle Control (CMC), provided experimental position data is supplied to the model. Inverse kinematics describes the process of calculating the angles of joints based on known position data of specific locations on the body. OpenSim retrieves experimental marker data (e.g., motion capture or inertial measurement units) and changes the position of the model to reflect the marker data by minimizing a sum of weighted squared errors of the markers (SimTK, 2020c). Inverse dynamics uses recorded motion kinematics and kinetics to calculate the net forces and torques at a particular joint for that movement by solving for Newton’s Second Law of Motion: $F = ma$ (SimTK, 2020b).

To reduce the risk of propagating errors between the experimental markers and modeled motion, OpenSim uses a tool called Residual Reduction Algorithm (RRA) that adjusts the calculated subject center of mass and IK to more closely resemble experimental GRF data (SimTK, 2020d). This process prevents residuals, which OpenSim defines as “large compensatory forces” that arise from discrepancies between experimental markers and resulting modeled motion (SimTK, 2020d). Following RRA, Computed Muscle Control (CMC) calculates the magnitude of excitations of desired muscles and muscle groups in order to create muscle-driven models for a particular motion. These muscle-driven models calculate the muscular forces required to complete a specified kinematic pattern.

In addition to kinematics, dynamics, and muscle-level excitation, metabolic probes provide a method to predict metabolic power expenditure for modeled muscles. Umberger et al. developed such an energy expenditure model (Umberger, Gerritsen, & Martin, 2003), (Umberger, 2003) that was used by OpenSim to develop a metabolic probe that can record model vector measurements to characterize muscle metabolic power (SimTK, 2020e).

OpenSim users generally follow the simplified pipeline depicted in Figure 3-19, beginning with experimentally collected ambulation data and ending with the desired analysis (i.e., joint moments, metabolic cost, etc.).

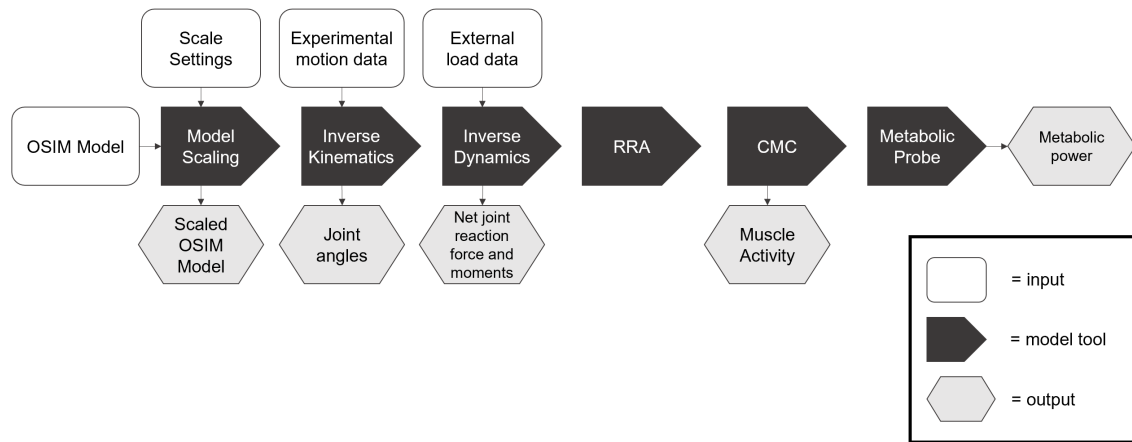


Figure 3-19: OpenSim gait pipeline.

This pathway for dynamic simulation was leveraged to investigate the impact of varied stiffness prescription on locomotion mechanics over in Earth and Lunar gravity environments.

3.3.2 Soft Knee Exoskeleton Stiffness and Model Integration

The soft knee exoskeleton was designed to exert a tunable magnitude of stiffness upon flexion of the knee. Bending of the exoskeleton would result in elastic energy storage that would aid in rebounding leg extension during gait. This behavior can be compared to a torsional spring, which is an elastic and flexible spring that exerts a moment in the direction opposite to the direction it is pulled; as the simple diagram in Figure 3-20 depicts, the magnitude of this moment increases as the pulling

displacement distance increases. Therefore, the soft knee exoskeleton was modeled in OpenSim as a torsional spring. An example of such a modeled torsional spring can be found in the OpenSim documentation (SimTK, 2020f).

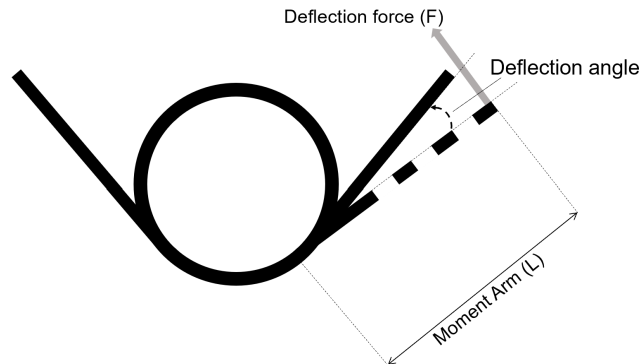


Figure 3-20: Simple diagram of a torsional spring with a deflection force (F) applied from a distance between the force and the spring center (L) to create a moment.

A torsional spring can be modeled at the knee in Python using the function `CoordinateLimitForce`, which imposes restrictions on the joint range of motion. A spring and damper are modeled to stop the coordinate range at the desired joint. When the joint coordinate approaches the limit, the spring and damper are smoothly engaged. The torsional spring properties are as follows:

- `upper_stiffness`: This is the stiffness of the knee spring assist during knee extension [Nm/deg]
- `upper_limit`: The spring is engaged when the knee angle is greater than this defined degree (extension) [deg]
- `lower_stiffness`: The `CoordinateLimitForce` will also generate forces preventing excess knee flexion [Nm/deg]
- `lower_limit`: Allow the full range of flexion motion [deg]
- `lower_limit`: Allow the full range of flexion motion [deg]
- `Damping`: A small damping term

- Transition: This term dictates the transition from zero to constant stiffness as the coordinate exceeds its limit (upper or lower), in degrees

These model parameters are listed in Table 3.3 with each simulation condition to be tested.

Table 3.3: Defined parameters for torsional spring model simulation conditions.

Parameter	Exo 1	Exo 2	Exo 3
Pressure [kPa]	30	50	90
Upper stiffness [Nm/deg]	0.089	0.176	0.324
upper limit [deg]	10	10	10
lower stiffness [Nm/deg]	0.089	0.176	0.324
lower limit [deg]	-18	-18	-18
damping	0.01	0.01	0.01
transition [deg]	2	2	2

3.3.3 Unassisted vs. Assisted Simulated Walking in 1G

Upon integration of the modeled soft knee exoskeleton stiffness in the form of a torsional spring, unassisted and assisted simulations of walking in 1G were performed. As mentioned in section 3.1.1., a sample experimental data set (marker trajectories, center of mass motion, and ground reaction forces) provided by OpenSim to accompany the Gait2392 model. The subject from whom the sample data is collected has a recorded weight of 72.6 kg and a height of 1.803 m. For the unassisted test case, a sample file containing a static trial was used to scale the model to the subject data. IK, ID, RRA, CMC, and Umberger 2010 metabolic probe analysis were performed following the OpenSim gait pipeline shown in Figure 3-21.

To simulate knee exoskeleton assisted walking in 1G, the torsional spring, which would model the stiffness exerted by the soft knee exoskeleton, was built via Python scripting (based on the example found here: (SimTK, 2020f)) and imported into the OpenSim Gait2392 model. Three testing conditions were simulated, with parameters identified in Table 3.3. These conditions reflect the three measured stiffness values of

1G Condition

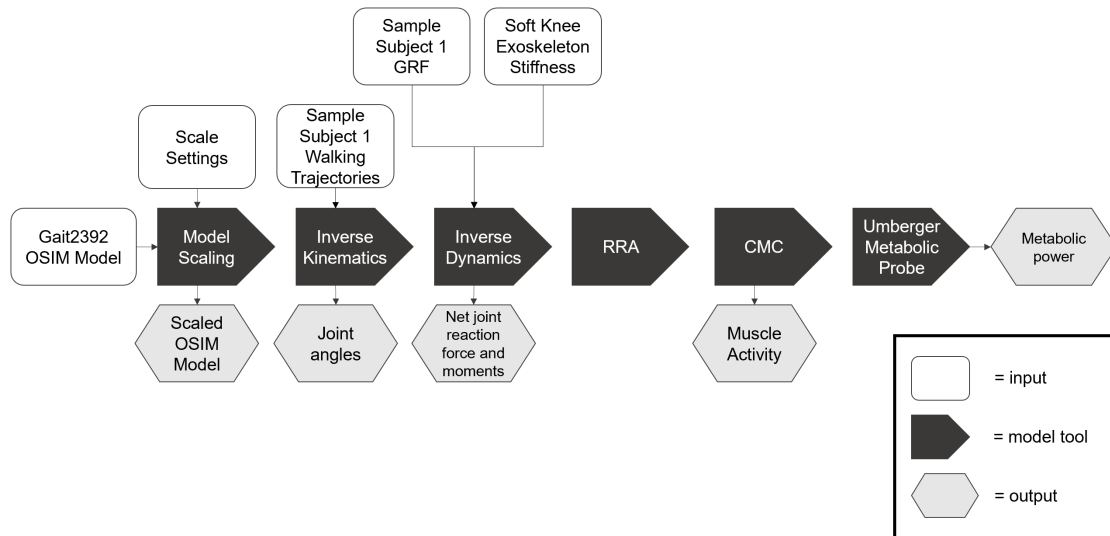


Figure 3-21: OpenSim gait pipeline for 1G condition.

the soft knee exoskeleton corresponding with increasing levels of internal pressure of the air bag actuators. “Exo 1” reflects the smallest soft knee exoskeleton preliminary stiffness results. “Exo 2” and “Exo 3” reflect the middle and highest preliminary stiffness, respectively. OpenSim defines the knee joint to be at 0 degrees when the femur is parallel with the tibia, with a positive angle change in extension and a negative angle change in flexion.

In both the unassisted and knee exoskeleton assisted conditions, CMC and the Umberger metabolic probe were applied to investigate the muscle force and metabolic cost by the total body and several muscle groups to compare the simulation results between these muscles for the unassisted and knee exoskeleton assisted conditions. The Gait2392 model includes 76 muscles in the lower body and torso. The muscles specifically associated with knee extension and flexion are as follows:

- Knee Extension Muscles:
 - Rectus Femoris
 - Vastus Medialis
 - Vastus Intermedius
 - Vastus Lateralis

- Knee Flexion Muscles:
 - Semimembranosus
 - Semitendinosus
 - Biceps Femoris: Long Head
 - Biceps Femoris: Short Head
 - Sartorius
 - Gracilis
 - Medial Gastrocnemius
 - Lateral Gastrocnemius

Actuation force and metabolic cost were calculated for the total body, knee flexion muscle group, and knee extension muscle group. These muscles are labeled in Figure 3-22.

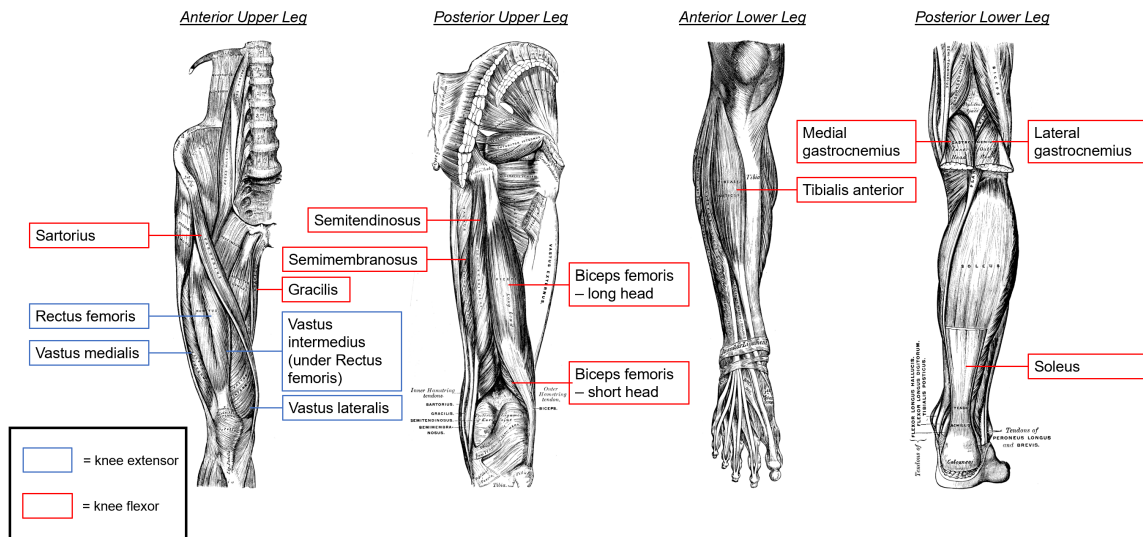


Figure 3-22: Muscles associated with knee extension (blue) and knee flexion (red) included in the OpenSim2392 model. Images adapted from: (H.Gray, 1913).

3.3.4 Unassisted vs. Assisted Walking in Partial Gravity

One of the roles of the NASA JSC ABF is to assesses the performance of space suits while subjects perform various tasks in order to evaluate ergonomics and occupa-

tional biomechanical impacts on the user (NASA, 2011). The ABF group performed Integrated Suit Testing in 2009 for unsuited subjects using the NASA Partial Gravity Simulator (POGO). POGO uses servos, air bearings, and gimbals to simulate partial gravity for use in EVA training for astronauts (NASA, 2020). Figure 3-23 depicts the POGO system with an astronaut performing a treadmill locomotion task for an EVA study (NASA, 2020).



Figure 3-23: A subject performing a treadmill locomotion task using the POGO partial gravity simulator during an EVA study (NASA, 2020).

ABF used POGO in conjunction with a treadmill equipped with ATMI force plates (Noraxon U.S.A., Inc., Scottsdale, AZ) and a VICON marker motion capture system to collect kinematic and kinetic walking data at varying speeds and inclines (Norcross & Clowers, 2010). GRF profiles were collected at 1000 Hz and VICON marker data were collected at 100Hz. The POGO system simulated 0.17G during these trials,

which is equivalent to lunar gravity. From these trials, marker trajectories, ground reaction force components and center of pressure (COP) coordinates were collected. For evaluation of the soft knee exoskeleton model at 0.17G, the selected NASA subject trial specified 1.9 mph walking speed over a flat surface. The subject had a mass of 81.6 kg.

Once the experimental data were retrieved from ABF, several processing steps were performed to ensure that the data would be compatible with OpenSim. The force plate axes were in conventional lab orientation (X is forward, Y is left, and Z is up); to correspond with the OpenSim standard engineering coordinate system (X is forward, Y is up, and Z is right), the experimental data was rotated to align with the OpenSim coordinate system. The files containing the GRF/COP and marker trajectory data were converted to OpenSim compatible formats (.mot and .trc, respectively). These processing steps were performed in MATLAB (The Mathworks, Inc., Natick, MA). By using the Scale Tool, experimental markers corresponding with bony landmarks were placed on the OpenSim Gait2392 model. The model and markers are depicted in Figure 3-24.

Due to the test subject's similar anthropometrics as the Gait2392 model, the model was not scaled to the experimental marker data. Upon placement of markers on the model using static trial data, marker RMS error = 0.0241741 m and marker max error = 0.04739 m. Desired error values are traditionally near or below RMS = 2 cm and max = 4 cm; the errors from the static trial were considered reasonable. Inverse kinematics were performed using the Inverse Kinematics tool for the knee and ankle for the 0.17G unassisted condition. Upon analysis of the experimental GRF data for the 0.17G condition, it became apparent that the subject repeatedly stepped on the interface between the center line of the force plate system. Due to the OpenSim requirement for importing GRF as separate left and right foot loading profiles, ID and actuation force analysis could not be performed for the 0.17G testing conditions from the available data. Consequently, without GRF data, RRA was not necessary to reduce discrepancies between the inverse kinematics and GRF. Actuation Force could not accurately be calculated for the 0.17G conditions.

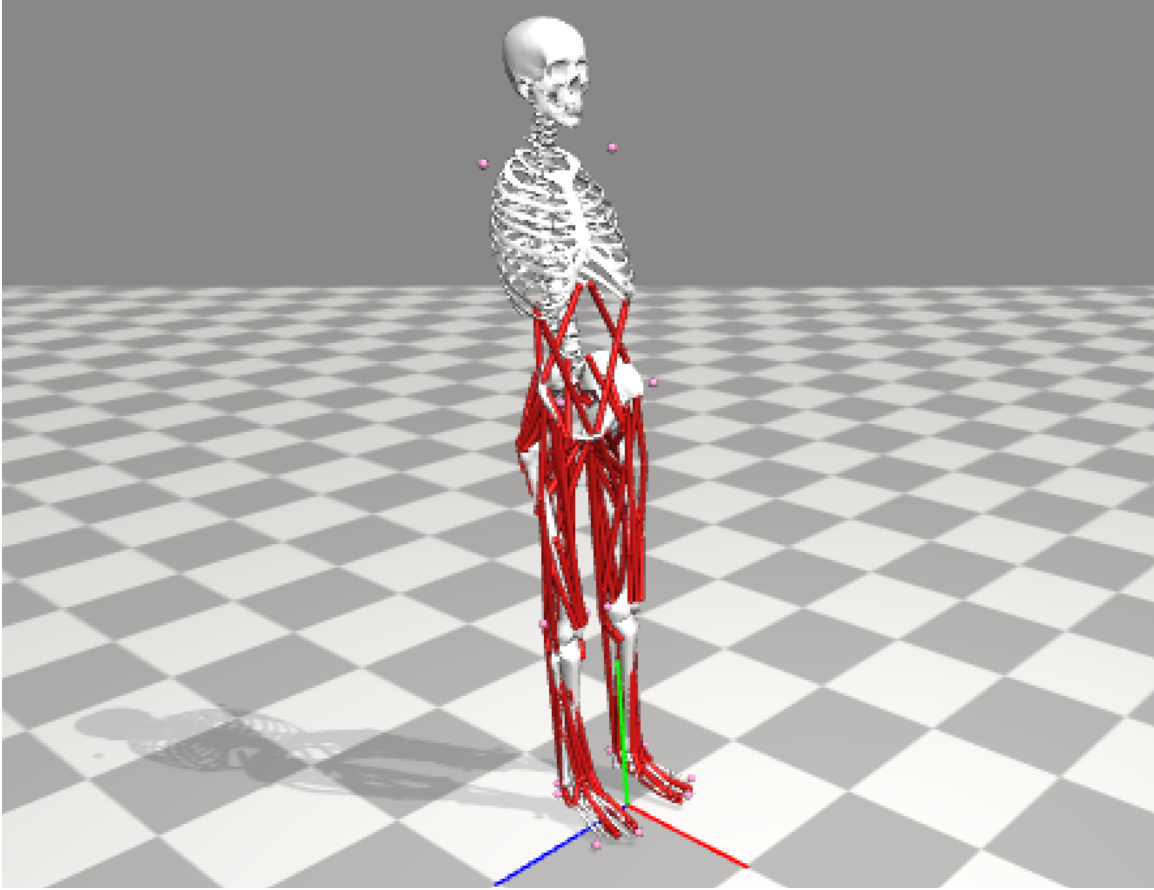


Figure 3-24: Gait2392 model with experimental markers (pink) aligning with NASA POGO trials.

Identically to the 1G conditions explained in sections 3.1.1 and 3.1.2, each of the 0.17G test cases included CMC/metabolic probe analysis, producing metabolic cost calculations for the total body, the knee flexion muscle group, and the knee extension muscle group. The analysis followed the OpenSim gait pipeline shown in Figure 3-25. The modeled soft knee exoskeleton stiffness was implemented via the same torsional spring Python script as the 1G cases, and three testing conditions (corresponding to increasing stiffness of the soft knee exoskeleton as the air bag are inflated to increasing internal pressures) were simulated, with parameters identified in Table 3.3

The same knee flexion and knee extension muscle groups were investigated to evaluate metabolic expenditure in 0.17G.

In this chapter, design criteria were established and fabrication techniques for the prototype knee sleeve were explored. Air bags were constructed using CAD and

Partial G Condition (1/6G)

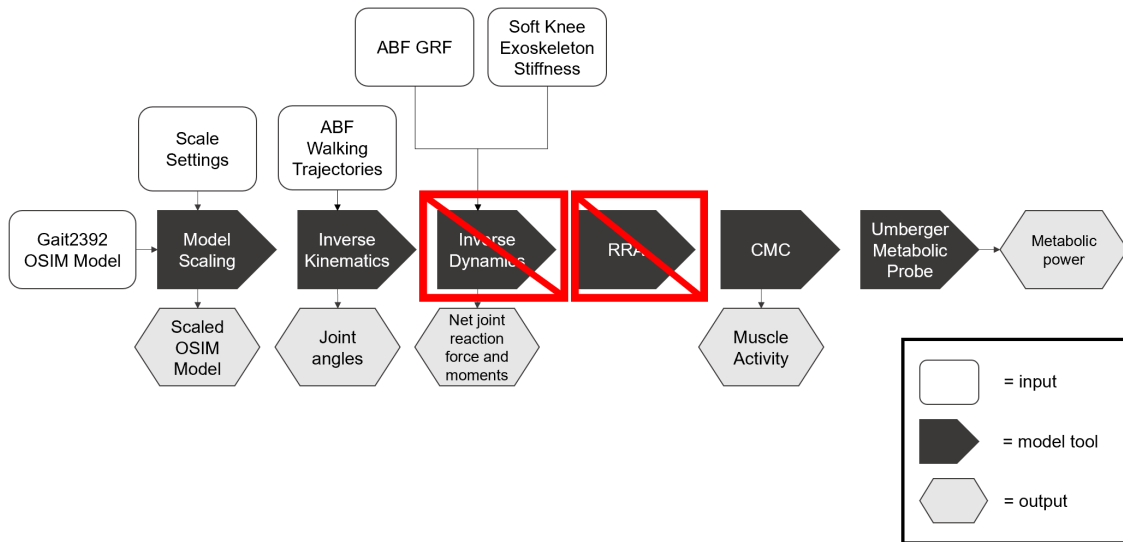


Figure 3-25: OpenSim gait pipeline for 0.17G condition.

WholeGarment knitting to exert the desired knee stiffness in parallel with the knee. OpenSim exoskeleton and musculoskeletal modeling methodology was described, including the use of the OpenSim2932 lower-body model and sample walking data to generate a muscle-driven simulation. These simulations included a torsional spring model with parameters designed to align with the anticipated stiffness behavior of the soft knee exoskeleton. Exoskeleton conditions were modeled in 0.17G and 1G for three degrees of stiffness corresponding to three magnitudes of airbag internal air pressures. Chapter 4 will discuss the final soft knee exoskeleton prototype and OpenSim 1G and 0.17G simulations to evaluate exoskeleton impacts on gait energetics.

Chapter 4

Results

A final knee exoskeleton prototype was produced from the methods described in Chapter 3. Additionally, simulations were run that modeled unassisted walking and three exoskeleton conditions that correspond with increasing levels of torsional spring stiffness at the knee, analogous to anticipated stiffness behavior of the final soft knee exoskeleton prototype. The following chapter describes the results of these methods.

4.1 Final Soft Knee Exoskeleton Prototype

A process was developed for producing three iterations of a soft exoskeleton knee sleeve prototype that can contribute to MCP. As the airbags are maximally inflated, shown in Figure 4-1, stiffness in parallel to the knee is exerted. The inflation is held constant by closing the air flow valve on the air source. Therefore, continuous power is not required to maintain inflation.

The stiffness exerted on the knee by the soft knee exoskeleton is dependent on the air bag internal pressure. When worn and fully inflated, the knee can be flexed approximately 50 degrees from full, standing extension before the user finds the soft knee exoskeleton stiffness too difficult to continue flexion. However, when the airbag is inflated to submaximal pressure, the user can easily bend the knee to approximately 90 degrees. As the internal pressure of the air bags is increased, the knee is aided in extension movement.



Figure 4-1: Soft knee exoskeleton V2 donned and maximally inflated anterior (left) and lateral (right) views.

A mechanical leg model with a knee hinge and force sensing cells was used to calculate preliminary stiffness values for three levels of inflated pressure. The testing protocol was completed by the D-Air Lab in Vicenza, Italy. These values were reported in Section 3.2 and are listed again here in Table 4.1.

Table 4.1: Preliminary stiffness value and maximum torque at 45 degrees for each soft knee exoskeleton inflated pressure. Adapted from D Air Lab measured results.

Nominal Pressure [kPa]	Preliminary Stiffness [Nm/deg]	Moment at 45 deg [Nm]
30	0.089	4.005
50	0.176	7.92
90	0.324	14.58

Clo 3D Fashion Design Software (New York City, NY) was employed to generate a 3D CAD model with the desired design updates. These updates were implemented in fabrication of the V3 prototype, shown in Figure 4-2. The updated V3 prototype improved the fit by decreasing the circumference in the distal cuff, lengthening of sleeve, and increased tapering around the knee. Additionally, the convolute joint present in the V2 prototype was eliminated by rotating the orientation of the air bags from horizontal to vertical.



Figure 4-2: Soft knee exoskeleton V3 donned and maximally inflated anterior (left) and lateral (right) views.

4.2 Modeled Knee Stiffness in 1G and 0.17G

OpenSim was used to model the effect of three Exo Conditions with increasing stiffness for each condition. These stiffness values are listed in Table 3.3 using the pipelines depicted in Figures 4-3 and 4-4. The three Exoskeleton conditions and unassisted condition were simulated for 1G (using OpenSim sample walking data) and 0.17G using NASA POGO simulated reduced gravity for a subject walking at 1.9 mph over a flat surface. This section reports the results of this analysis. Each plot depicts the conditions listed in Table 3.3, referred to as “Unassisted”, “Exo 1”, “Exo 2”, and “Exo 3”.

4.2.1 Joint Kinematics and Moments in 1G and 0.17G

Joint angles were plotted for the knee and ankle for the 1G and 0.17G conditions in Figure 4-5. OpenSim defines the ankle joint to be at 0 degrees when ankle is at a 90 degree angle with the tibia (such as when static standing), with a positive angle change in dorsiflexion and a negative angle change in plantarflexion.

The method used to model knee stiffness as a torsional spring imparts the desired stiffness constraints at the specified angle displacements, but the model continues to perform the full gait cycle. Therefore, the joint kinematics do not change between the

1G Condition

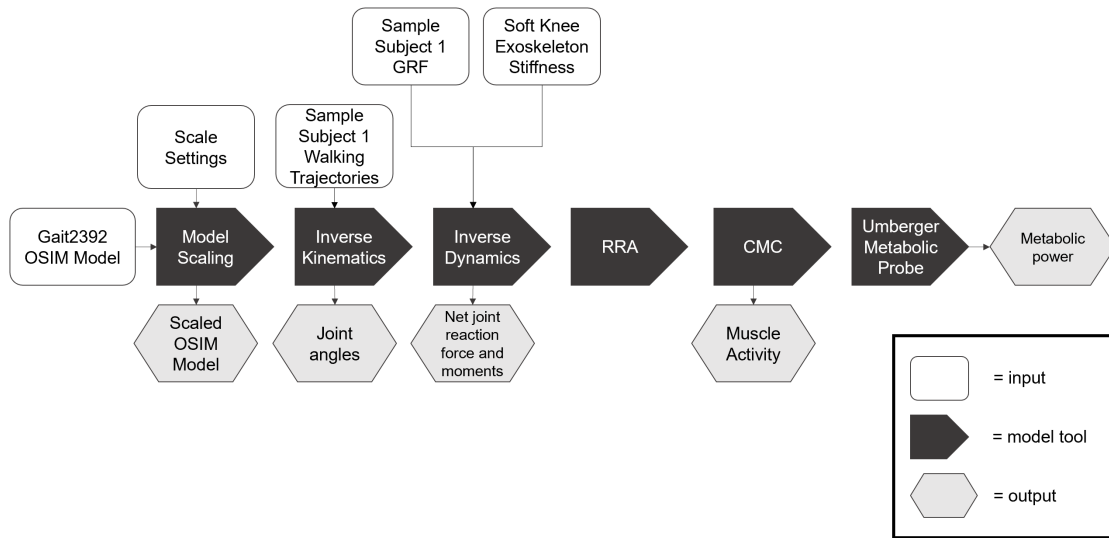


Figure 4-3: OpenSim gait pipeline for 1G condition.

Partial G Condition (1/6G)

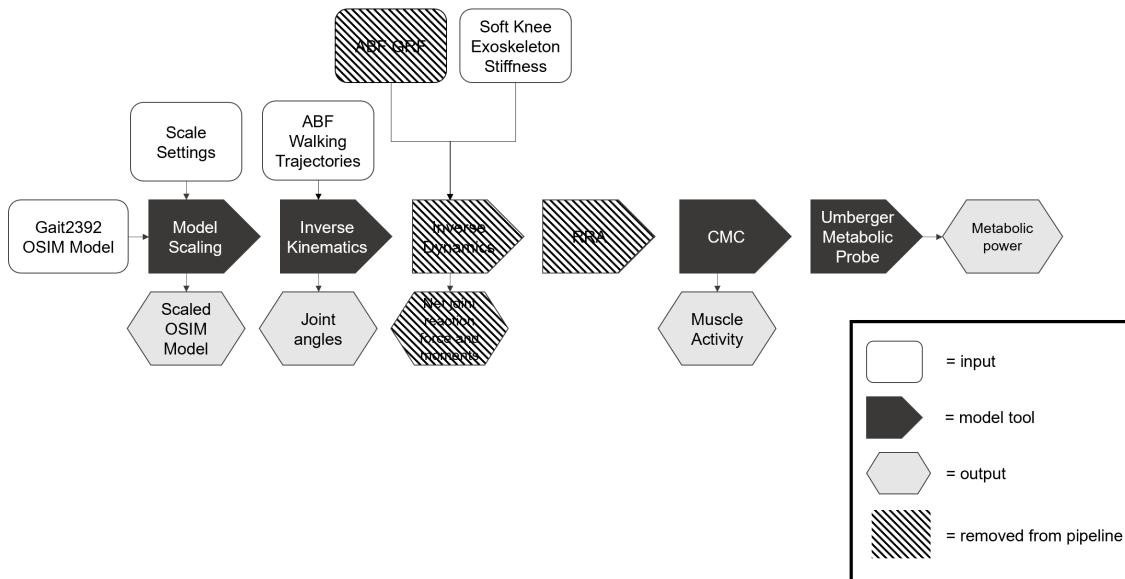


Figure 4-4: OpenSim gait pipeline for 0.17G condition with removed tool steps (Inverse Dynamics and RRA) and model outputs (Net joint reaction force and moments) that could not be performed with available GRF data.

Unassisted or Exoskeleton conditions and were not plotted. Compared to the 1G case, the 0.17G knee angle shows a smaller maximum knee flexion angle, through there is a larger maximum knee angle occurring at full extension. The 0.17G case for the ankle shows a larger maximum angle achieved during plantarflexion and a decreased

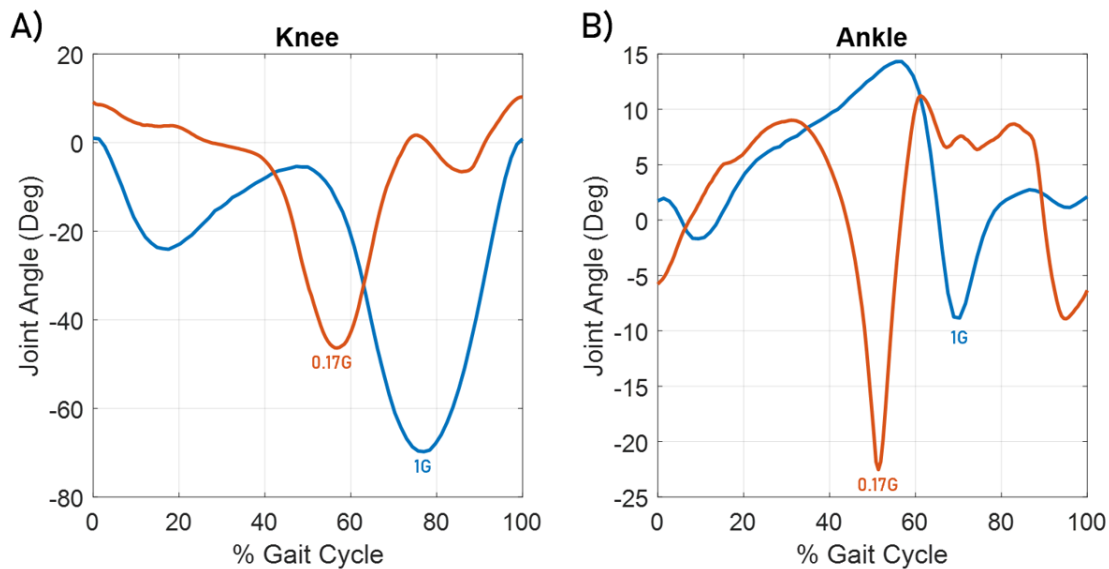


Figure 4-5: A) Knee and B) ankle joint angles resulting from inverse kinematics of 1G and 0.17G marker trajectories.

maximum dorsiflexion angle. Subject walking speed was slower in the 0.17G case compared to the 1G case, resulting in a phase shift in joint angles between the 0.17G and 1G cases.

As described in section 3.3.4, inverse dynamics could not be performed with the available GRF and COM data. Therefore, joint moments were only calculated for the 1G condition and plotted in Figure 4-6. The joint moment in Figure 4-6 is normalized with respect to the Unassisted condition. Exo 1, 2, and 3 did not alter the knee moment for a majority of the gait cycle. During peak flexion, Exo 1, 2, and 3 reduced knee moment as the increasing stiffness of Exo 1, 2, and 3, respectively.

4.2.2 Muscle-Driven Model Comparison to Unassisted Walking Model

OpenSim features the capability to dynamically analyze the required force to actuate any muscle of the model as part of the CMC tool. Figure 4-7 depicts this actuation force for the knee flexion and knee extension muscle groups in 1G for each Unassisted and Exo condition. Without GRF profiles, actuation force could not accurately be

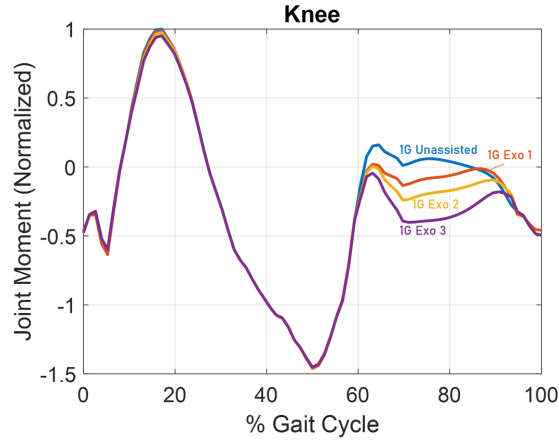


Figure 4-6: Knee moment resulting from inverse dynamics of 1G GRF and marker trajectory data.

calculated for the 0.17G conditions. From Figure 4-7, it appears that increasing stiffness in Exo 1-3 leads to increased knee flexion actuation force occurring during flexion and a decreased knee extension actuation force during extension. Each actuation force plot is normalized relative to the 1G Unassisted condition for ease of comparing the effect of the Exo conditions to the Unassisted simulation.

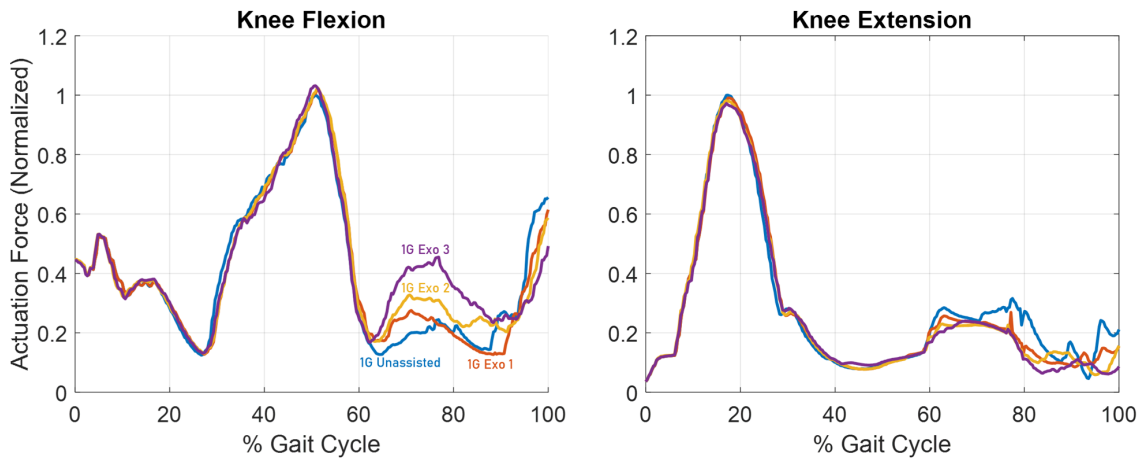


Figure 4-7: A) Knee Flexion and B) Knee Extension actuation force for Unassisted, Exo 1, Exo 2, and Exo 3 during 1G walking. Actuation force is normalized relative to the Unassisted condition.

As described in Section 3.3.1, the 2010 Umberger metabolic probe was utilized in conjunction with the CMC tool to estimate metabolic consumption of individual muscles necessary to complete a specified kinematic movement. For both 1G and 0.17G

conditions, the IK results from the experimental motion capture marker trajectories were specified as the kinematic movement for evaluation of metabolic expenditure. In the 1G case, the GRF profile was included in the CMC analysis. The Unassisted and Exo conditions were evaluated the knee flexion and knee extension muscle groups, as well as total body metabolic cost. Each of these plots in Figures 4-8 and 4-9 depicts a cumulative metabolic consumption as the gait cycle is completed. Again, these metabolic cost plots are normalized relative to the Unassisted condition to compare the effect of each Exo Condition to the Unassisted condition for a given gravity level.

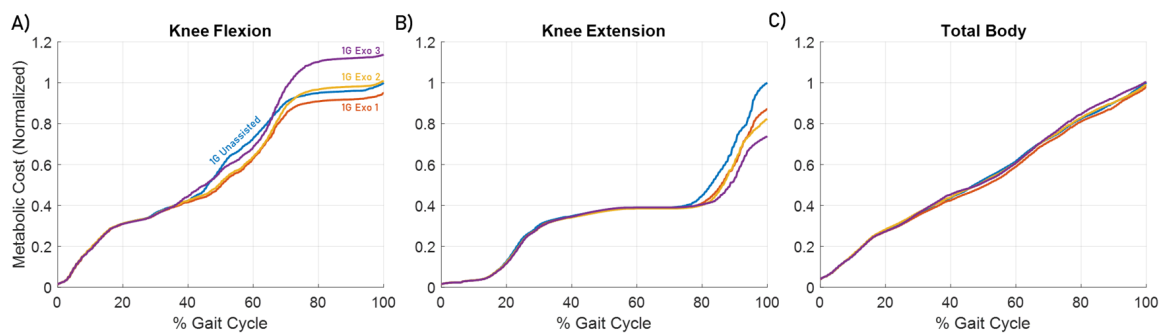


Figure 4-8: 2010 Umberger Metabolic Probe analysis in Unassisted, Exo 1, Exo 2, and Exo 3 conditions for A) Knee Flexion, B) Knee Extension, and C) Total Body muscle groups in 1G. Metabolic cost is normalized relative to the Unassisted condition.

The 1G cases in Figure 4-8 show a general increase in knee flexion metabolic cost, but a decrease in knee extension metabolic cost corresponding with the stiffness increase associated with sequential Exo conditions.

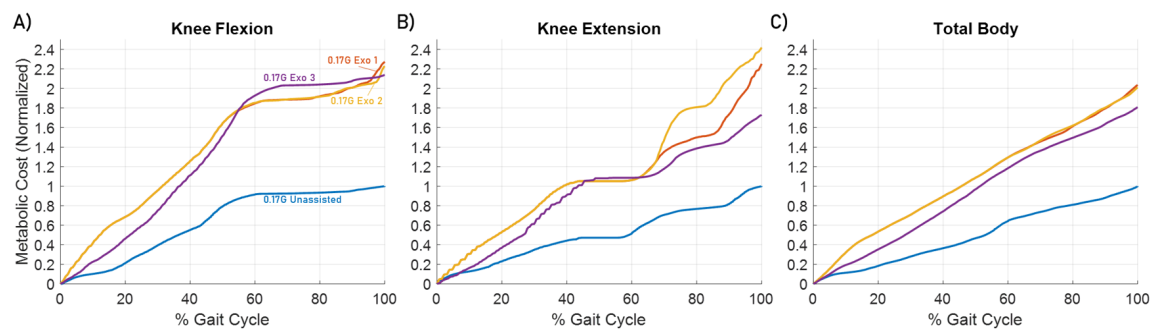


Figure 4-9: 2010 Umberger Metabolic Probe analysis in Unassisted, Exo 1, Exo 2, and Exo 3 conditions for A) Knee Flexion, B) Knee Extension, and C) Total Body muscle groups in 0.17G. Metabolic cost is normalized relative to the Unassisted condition.

During the 0.17G simulations in Figure 4-9, there is a general increase in both

knee flexion and knee extension metabolic cost, as well as a noticeable increase in total body metabolic cost compared to the Unassisted condition.

4.2.3 Test Condition Peak Values

From the simulation data plotted in Figures 4-6, 4-7, 4-8, and 4-9, peak values were extracted for: knee moment, knee flexion metabolic cost and actuation force, knee extension metabolic cost and actuation force, and total body metabolic cost. These values are listed in Table 4.2.

Table 4.2: Peak moment, metabolic cost, and actuation force values for Exo 1, 2, and Exo 3 during A) 1G and B) 0.17G. Each value is normalized relative to the Unassisted case in the corresponding gravity level.

A)		<i>Relative to 1G Unassisted</i>		
1G		Exo 1	Exo 2	Exo 3
Peak Knee Moment		0.989	0.975	0.951
Total Knee Flexion Metabolic Cost		0.949	1.010	1.138
Total Knee Extension Metabolic Cost		0.991	0.981	0.972
Total Body Metabolic Cost		0.979	0.991	1.005
Peak Knee Flexion Actuation Force		1.019	1.023	1.032
Peak Knee Extension Actuation Force		0.991	0.981	0.972
B)		<i>Relative to 0.17G Unassisted</i>		
0.17G		Exo 1	Exo 2	Exo 3
Peak Knee Moment				
Total Knee Flexion Metabolic Cost		2.274	2.228	2.138
Total Knee Extension Metabolic Cost		2.252	2.418	1.729
Total Body Metabolic Cost		2.037	2.010	1.808
Peak Knee Flexion Actuation Force				
Peak Knee Extension Actuation Force				

This chapter demonstrated the final prototype, preliminary measured stiffness, and range of motion afforded by the soft knee exoskeleton. A pipeline was outlined using OpenSim software that uses motion capture walking trajectories and ground reaction force profiles to scale a model, perform inverse kinematics, inverse dynamics, RRA, CMC, and run the 2010 Umberger metabolic probe. This pipeline was used for Earth gravity and adapted for Lunar gravity. The following chapter will assess the extent to which the soft knee exoskeleton met its design criteria and the capabilities of the model pipeline. The simulations of joint angles, joint moments, muscle actuation force, and metabolic expenditure for each soft knee exoskeleton stiffness condition in varied gravity will be evaluated and impacts will be reviewed relative to the literature.

Chapter 5

Discussion

This thesis summarizes the design and development of prototype actuation for a soft exoskeleton, in collaboration with the D-Air Lab (Vicenza, Italy). The following design criteria were established to guide the design of this soft exoskeleton:

1. The soft knee exoskeleton method of articulation shall provide stiffness in parallel with the knee.
2. The soft knee exoskeleton method of articulation shall provide rotational stiffness to hinder knee flexion.
3. The soft knee exoskeleton shall provide adjustable levels of stiffness.
4. The soft knee exoskeleton stiffness actuation shall minimize power drawn from suit reserves.
5. The soft knee exoskeleton shall not diminish the MCP provided by the BioSuit™.

Additionally, a pipeline was established to evaluate simulations of passive soft knee exoskeleton stiffness in partial gravity. This pipeline enabled computational analysis of stiffness at the knee impacts on knee flexion and extension, as well as total body metabolic cost.

5.1 Contributions

The main goal of this thesis was to develop and evaluate prototype actuators in a soft knee exoskeleton that can apply adjustable stiffness to the knee while permitting full range of motion for flexion and extension. Additionally, this fabrication method of this sleeve required the inclusion of the capability to aid in producing sufficient mechanical counterpressure for safe use in space.

The development of these prototype sleeves is vital in optimizing the trade-off between maximized locomotion efficiency in reduced gravity and minimized metabolic expenditure associated with locomotion and space suit inflexibility. The integration of knee and arm soft exoskeleton sleeves into the BioSuit™ will inform future space suit design to enable longer, safer, and more complex EVAs in partial gravity.

The following two specific research aims were pursued to develop and assess the performance of tuned knee stiffness in partial gravity:

- Specific Aim 1: Develop a prototype tunable knee stiffening sleeve for soft exoskeleton.
- Specific Aim 2: Investigate the impact of varied stiffness prescription on locomotion mechanics and metabolic consumption in Earth and Lunar gravity using computational simulation of walking.

5.1.1 Hypothesis and Specific Aim 1

HYPOTHESIS 1: WholeGarment knitting can be employed to develop a prototype tunable knee stiffening sleeve and provide hoop stress to provide MCP. This fabrication method will also provide future integration of LoNE patterning. Integrated airbag technology can exert a range of stiffness which provides varying opposition to flexion during locomotion.

Design and fabrication of a soft knee exoskeleton that can apply adjustable stiffness to the knee while permitting full range of motion for flexion and extension was demonstrated. Additionally, we illustrated the capability of WholeGarment knitting

to aid in producing sufficient mechanical counterpressure for safe use in space. Clo 3D Fashion Design Software (New York City, NY) was employed to generate a 3D CAD model with design updates, which were then realized in the fabrication of the soft knee exoskeleton V3. These updates improve the overall fit and eliminate convolute joints present in the soft knee exoskeleton V2. Stiffness can be modulated via the level of air bag internal pressure.

This thesis builds upon the investigations by Carr and Newman, who found that there could be elastic energy storage benefits to joint torques (Carr & Newman, 2017), and preliminary data has shown that low-magnitude stiffness significantly increases calculated net energy recovery when compared to high-magnitude stiffness (Carr & Newman, 2007). This soft knee exoskeleton will also advance next generation space suit development and inform how knee joints can be optimally actuated to aid in metabolic cost minimization, such as the work being performed by Diaz-Artiles et al. with active robotic knee actuation at the knee joint of the EMU (Diaz-Artiles et al., 2020). Additionally, soft knee actuation development contributes to the efforts to build a soft exoskeleton that actuates via pneumatics, including the work of Wehner et al. (Wehner et al., 2013). Knowledge of how soft knee exoskeleton stiffness impacts energetics during ambulation will aid in reducing metabolic cost using soft exoskeletons, which is an active field of human performance augmentation research (Asbeck et al., 2015), (Lee et al., 2018).

The soft knee exoskeleton developed in this paper will further our limited understanding of how tuned joint torques could optimize partial gravity locomotion energetics. The exoskeleton will be leveraged to investigate the cost-benefit of energy storage versus metabolic expenditure related to knee joint torques. Additionally, by developing space suit knee joints that are less stiff than existing suits, trauma caused by suits may be reduced in the lower body. Lower-body muscle groups, such as the quadriceps, thighs, gluteal muscles, and lower back were reported by users to experience the greatest amount of discomfort and muscle fatigue in the Mark III Advanced Space Suit Technology Demonstrator EVA Suit during and EVA Walkback Test performed by NASA (Norcross & Clowers, 2010).

Development of a soft knee exoskeleton that can aid in producing MCP build upon the work by Newman and others to produce an engineering prototype of the BioSuitTM (Newman et al., 2005). WholeGarment knitting was demonstrated as a method to increase donning/doffing problems associated with MCP (Anderson, 2011), (Judnick et al., 2010), as well as include the potential to integrate LoNEs (such as those calculated by Newman, Obropta, and Wessendorf (Obropta & Newman, 2015), (Obropta & Newman, 2016), (Wessendorf & Newman, 2012)).

Reducing injury risk and determining how human metabolic expenditure is minimized by alterations in joint stiffness in reduced gravity would benefit not only development of MCP technology (such as the BioSuitTM), but also improve design requirements for gas-pressurized space suits that are less metabolically expensive than current space suit models.

5.1.2 Hypothesis and Specific Aim 2

HYPOTHESIS 2: A soft knee exoskeleton can be modeled as a torsional spring stiffness at the knee via OpenSim software (Stanford, Palo Alto, CA). Gait mechanics, muscle forces, and estimated muscle metabolic expenditure can be compared between unassisted walking and assisted walking with an exoskeleton across in Earth and Lunar gravity using the OpenSim pipeline. Variable knee joint stiffness in an exoskeleton can allow for reduced metabolic cost in select gravity conditions during walking musculoskeletal model simulations.

From these simulations, it can be concluded that OpenSim capabilities enable torsional spring stiffness modeling at the knee analogous with predicted stiffness behavior of the soft knee exoskeleton. The chosen method of this stiffness modeling enables specification of upper and lower torsional spring stiffness, upper and lower joint angle limit, damping and transition terms. Integration of OpenSim sample walking data for 1G and NASA experimental Lunar gravity walking data provided the ability to compare calculated joint angles, joint moments, muscle actuation force, and metabolic expenditure between Exo conditions within each gravity level. By analyzing the trends of increasing torsional spring stiffness corresponding to sequential Exo

conditions, 1G metabolic cost associated with the knee extension muscle group decreased, while 1G knee flexion muscle group metabolic cost increased. These findings correlate with increased effort in flexing the knee during walking as a result of the stiffness provided by the soft knee exoskeleton in parallel with the knee, which was intended to resist flexion. The decrease in extension metabolic cost could correspond with increased elastic energy storage provided by the soft knee exoskeleton, aiding in rebounding leg extension during gait. A phase shift in knee and ankle kinematics was observed, due to a slower walking speed in the 0.17G condition compared to 1G. Conversely, in 0.17G, all Exo condition stiffness resulted in increased metabolic cost when compared to the Unassisted Condition. However, when comparing only the 0.17G Exo conditions, as stiffness increased, knee extension and total body metabolic cost appeared to decrease.

The modeling work outlined in this thesis demonstrates a promising methodology for quickly simulating joint angles, joint moments, muscle actuation force, and metabolic expenditure conditions across a gravity spectrum. This pipeline provides the capability to examine varying stiffness applied at the knee that reduces the cost and time associated with running full experimental trials, such as those performed by Carr and Newman (Carr & Newman, 2007), (Carr & Newman, 2008), (Carr & Newman, 2017). Computational simulation results plotted in Chapter 4 depict a general downward trend in 0.17G knee extension and total body metabolic cost in the Exo conditions as stiffness increased; therefore, higher magnitudes of stiffness at the knee exerted by a soft knee exoskeleton could continue to decrease these metabolic values. If so, further increase in knee exoskeleton stiffness could result in a decreased metabolic cost of knee extension and total body in Lunar gravity. Such models can also build upon the recent work by Kluis et al., who are also leveraging OpenSim to model active robotic assistance at the knee joint of the EMU (Kluis et al., 2020).

Additionally, this work contributes to the relatively sparse body of knowledge that currently exists involving analysis of metabolic cost and exoskeleton modeling for reduced gravity conditions. Models such as the one described in this thesis can be used to better understand astronaut locomotion energetics by simulating reduced

gravity and space suit conditions. These models can be validated against NASA EVA Walkback Tests performed by Norcross et al. (Norcross & Clowers, 2010), then used to extrapolate on novel EVA scenario impacts on astronaut metabolic cost. Understanding how a human interacts with a soft knee exoskeleton in a partial gravity environment could help identify how to decrease unwanted joint moments and muscle forces. This knowledge supplements prior human-suit interaction investigations (such as those performed by Stirling, Arezes, and Anderson (Stirling et al., 2019)) and a validated model can aid in EVA planning that reduces risk of injury and/or overexertion.

5.2 Challenges and Limitations

Preliminary results showed that the soft knee exoskeleton can apply adjustable stiffness in parallel to the knee and resist motion during knee flexion. Additionally, the exoskeleton does not require continuous power to maintain inflation while worn, therefore minimizing power usage. Finally, the airbags of the exoskeleton are directly integrated with the base fabric; once inflated, the airbags provide increased mechanical pressure onto the skin. Therefore, all five design criteria for the soft knee exoskeleton were met.

It should be noted that when the airbag is worn by users with diverse knee strengths, it may be difficult to determine the optimal air pressure of the airbags to exert the desired stiffness. In order to alleviate this challenge, further airbag designs will include partitions within the airbags that allow portions of the airbag to be inflated independently. The exoskeleton airbags could then be inflated to discrete pressures that enable prescribed stiffness across a continuum of knee flexion strength. Additionally, we had difficulty maintaining constant airbag pressure. This issue was due in part to the lack of reliable air pressure measurement during data collection and the absence of a sufficient method of air pressure regulation. In future iterations of the exoskeleton, reliable air pressure regulation will be included.

WholeGarment knitting was shown to be an effective method of fabricating a

customized garment with fibers and knitting techniques that provide desired material behavior. The WholeGarment knitting method used in this work requires significant upfront time expenditure in developing the digital knitting design. However, once the design is complete, the garment is knitted in a matter of hours. Additionally, small edits to iterate the design can be made quickly. Therefore, WholeGarment knitting can be considered advantageous for fabrication when the design team includes personnel with appropriate training and expertise. As mentioned above, one difficulty in the knitting process was that the Shima Seiki model SWG 091N used for fabrication of the soft knee exoskeleton did not have enough yarn guides to include the Spandex inlay that was used for the final base fabric prototype, shown in Figure 3-5. Including this Spandex inlay would likely significantly increase the mechanical counterpressure exerted by the soft knee exoskeleton. There are newer models of the Shima Seiki machine (such as the SWG 061N2 or SWG 091N2) that include a greater number of yarn guides; access to such a model will be pursued for future iterations of the soft knee exoskeleton that seek to increase the exerted mechanical counterpressure.

Several modeling limitations became apparent during this study. First, the parameters constraining the modeled torsional knee spring were established based on preliminary soft knee exoskeleton characterization data. Until more extensive behavior characterization testing occurs, exoskeleton locomotion impacts cannot be definitively predicted using this method of modeling.

Additionally, as described in section 3.3.4, due to discrepancies between data collection methodology and OpenSim input data constraints, the GRF and COM profiles for 0.17G walking could not be implemented into the modeling pipeline. One resulting limitation of this study is that ID and muscle actuation force were unable to be performed for the 0.17G test case. Since GRF files are also used for the CMC tool, the numerical values for simulated metabolic cost and actuation force are likely not accurate. To mitigate this limitation, each test condition was only compared within the corresponding gravity level. These simulations were also normalized relative to the Unassisted test condition. Therefore, metabolic cost of each Exo condition can be compared relative to each other to extract trends associated with increasing exerted

knee stiffness.

The small sample size for experimental subject data was a modeling limiting factor. These simulations describe the joint angles, joint moments, muscle actuation force, and metabolic expenditure impacts for a male subject of 72.6 kg (1G) or 81.6 kg (0.17G) - this is a very limited subject population. Differing subject anthropometrics, mass, sex, or age could impact the simulated results. Simulating a more diverse subject population would provide a more comprehensive view of soft exoskeleton impacts on locomotion for varying subject characteristics.

Finally, these simulations only included Earth and Lunar gravity levels. Humans are preparing for human missions to Mars, so we must include Martian gravity in future simulations to ensure astronauts are prepared for EVA in all prospective gravity conditions.

5.3 Future Work

In order to determine the impact of tuned knee stiffness on locomotion in reduced gravity, future work will include a human study evaluating how the soft knee exoskeleton influences the metabolic expenditure of the wearer in simulated partial gravity. As described previously, further iterations of the soft knee exoskeleton will be fabricated that have a partitioned airbag structure that will allow the exoskeleton to be inflated to defined, discrete levels of stiffness. The goal of the pending human study will be to characterize the effects of the final soft knee exoskeleton design with variable knee stiffness on the biomechanics and metabolic cost expenditure associated with locomotion in reduced gravity. To simulate reduced gravity in this exoskeleton, the Human Systems Laboratory at MIT houses a partial gravity offload system, called the Moonwalker. The Moonwalker uses a spring system to remove a customized percentage of the user's body weight, enabling the simulation of partial gravity. A wearable metabolic system will be employed to measure various parameters (such as maximum oxygen uptake) that represent metabolic expenditure, and motion capture will be employed for calculation of center of mass motion to measure energy expenditure per

step during walking and running.

Once the effects of tuned stiffness on metabolic expenditure are well understood, a control system and logic programming should be designed to regulate the inflation/deflation of the airbag system, as well as maintain a required airbag pressure that is customized to the user.

Knitting techniques will likely include active fibers, such as shape-memory polymers, that can aid in exerting the desired 29.6 kPa of MCP. Following development of a base fabric that can exert constant, sufficient pressure that is uniformly distributed, a longer duration human study will be performed to ensure that the interaction between the base fabric and airbags does not induce tissue edema, building upon the analysis performed investigating risk of edema associated with MCP (Carr & Trevino, 2019).

To increase the fidelity of this modeling methodology, future work will include conducting experimental trials with the soft knee exoskeleton where the subject wears a metabolic cart. The results of these experiments will validate the simulated metabolic estimates. The validated modeled that can then be applied with greater confidence to a broader gravity spectrum and stiffness prescription. In these experiments, the subjects will be directed to ensure that their strides do not land on the center line of the treadmill force plate system separating the left and right sides of the force plates. This experimental protocol specification will ensure compliance between GRF/COM data and OpenSim file requirements.

As mentioned above, future work will include more comprehensive behavior characterization of the soft knee skeleton; the modeled torsional knee spring will then be updated to better reflect this behavior.

In future modeling, the same subject marker trajectories will be used in both of the 1G and 0.17G conditions. Using the same subject for these analyses will allow joint angle, joint moment, muscle actuation force, and metabolic expenditure to be compared between gravity levels, as well as within gravity levels. Conclusion can then be drawn on the impact of gravity level on these measures, rather than only comparing between Unassisted/Exo conditions within a gravity level. Future experimental

subject pools will include a more diverse subject population that reflect expected soft knee exoskeleton and BioSuitTM users; active astronauts encompass a wide swath of anthropometrics, mass, and age, which are not currently accounted for in this modeling pipeline. EVA suits that optimize joint mechanics and muscle metabolic cost will likely be unique to each user, so a diverse subject population is necessary to establish prospective customized stiffness prescriptions. Future simulation scenarios will also include “loping” gait over inclined surfaces to better reflect partial gravity EVA.

To ensure that a robust investigation into the most beneficial exoskeleton can be performed, future modeling will include not only passive knee stiffness, but also actively controlled exoskeleton stiffness. Better understanding the potential impacts of deliberate timing of stiffness exertion in reduced gravity will provide insight into whether future MCP suits, such as the BioSuitTM would benefit from active knee stiffness control. Additionally, conducting kinematic, dynamic, and metabolic analyses of other joints involved in locomotion (i.e. ankle and hip) would help to discern whole body mechanical changes induced by isolated joint stiffness.

5.4 Conclusions

Computational modeling can be leveraged to evaluate the efficacy of tuned joint stiffness in partial gravity in a way that minimizes experimental time and financial expenses, leading to more efficient design and fabrication of a soft knee exoskeleton for use in space suits and EVAs. By developing a robust and novel soft knee exoskeleton that has tuned joint stiffness capabilities, this work seeks to help reduce required life-support consumables, enable excursions that traverse longer distances and varying terrain, maintain safety, and augment the performance of astronauts.

Appendix A

Appendix: Soft Knee Design and Fabrication

Table A.1: Leferon (Barcelona, Spain) technical data sheet for PA 6 78/24/2 polyamide yarn.

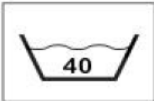
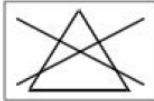
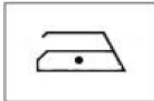

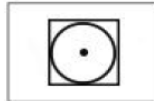
CARACTERISTICAS DESCRIPTIVAS					
Titulo comercial	PA 6 78/24/2				
Composición	Poliamida 100%	Ley 883/73			
Título	146 Decitex +/- 20%	UNI EN ISO 2060 Enero 1997			
Torsión	100 torsión por metro	UNI EN ISO 2061 Enero 1997			
Tangle	Procedimiento interno				
CARACTERISTICAS FISICAS					
Tenacidad G/D	4,30	UNI EN ISO 2062 Julio 1997			
Alargamiento	32,20%	UNI EN ISO 2062 Julio 1997			
Crimp	23,50%				
Encimaje	3,00%	Procedimiento interno			
CARACTERISTICAS TINTORIALES					
Degradación Descarga					
Luz artificial (xenontest)	2-5	ISO 105 B-02			
Agua	4-5	ISO 105 E-01			
Sudor acido	4-5	ISO 105 E-04			
Sudor alcalina	4-5	ISO 105 E-04			
Roce seco	4-5	ISO 105 X-12			
Roce húmedo	4-5	ISO 105 X-12			
Lavado húmedo 40°C	4-5	ISO 105 C-06			
Lavado seco	4-5	ISO 105 D-01			
Planchado seco 30seg/180°C		ISO 105 X-11			
CARACTERISTICAS COLORIMETRICAS					
	D65	A	F11	TL84	
Desviación s/master Leferon	1	1	1	1	CMC (2:1)
Exterior/Medio/Interior	1	1	1	1	CMC (2:1)
SIMBOLOS DE ETIQUETADO					
					
CERTIFICACIONES					
Oeko - Tex	Standard 100		N° 2004AN1251		
Reach	Productos utilizados en fase de preregistro				
CARACTERÍSTICAS EMBALAJE					
Dimensiones caja	600x400x490				
Peso máximo x caja	25kgr.				

Table A.2: Expotex (Stezzano, Italy) technical data sheet for CY 325-156 TP/Nylon thermoplastic coated yarn.

Product description		
CY 325-156 TPU/NYLON		
Thermoplastic coated yarn		

Technical data		
Nominal size	[mm]	0.325
	[dtex]	900
Core fiber		Nylon
Core size	[dtex]	156
Coat polymer type		TPU
Coating percentage	[%]	83
MVR (ISO 1133 - 160 °C/2.160 Kg)	[cm ³ /10 min]	13
Application temperature range	[°C]	120 - 150
Tenacity (UNI EN-ISO 2062/2010)	[cN/dtex]	0.7
Elongation at break	[%]	17.3
Bobbin type	Cone	L290 - D150 mm
Bobbin weight	[Kg]	0.9
Bobbin lenght	[m]	10000
Running lenght	[m/Kg]	11111

All data and recommendations are based on our present knowledge but are not binding.
 All indicated values have a tollerance of ± 5%.
 By: Technical Service Dept.
 All right reserved Expotex srl

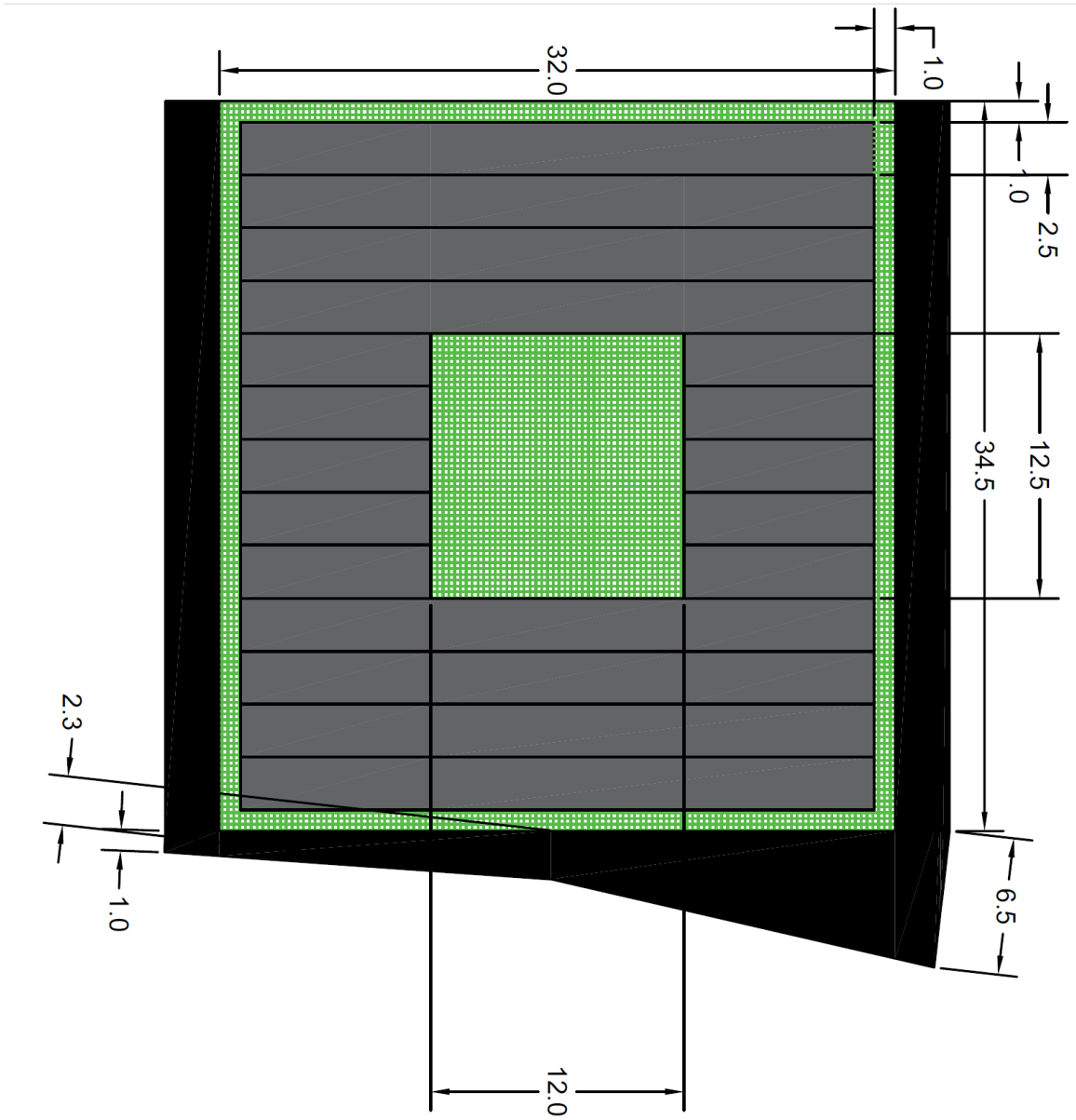


Figure A-1: CAD drawing of soft knee exoskeleton prototype V3 (dimensions in inches).

Appendix B

Appendix: OpenSim Modeling

Table B.1: Muscles present in the Gait2392 model. All muscles listed are included for both the left and right sides of the model.

OpenSim Gait 2392 Muscles
Gluteus Medius 1, 2, 3
Gluteus Minimus 1, 2, 3
Semimembranosus
Semitendinosus
Biceps Femoris-Long Head
Biceps Femoris-Short Head
Sartorius
Adductor Longus
Adductor Brevis
Adductor Magnus 1, 2 3
Tensor Fasciae Latae
Pectineus
Gracilis
Gluteus Maximus 1, 2, 3
Iliacus
Psoas Major
Quadratus Femoris
Piriformis
Rectus Femoris
Vastus Medialis
Vastus Intermedius
Vastus Lateralis
Medial Gastrocnemius
Lateral Gastrocnemius
Soleus
Tibialis Posterior
Flexor Digitorum Longus
Flexor Hallucis Longus
Tibialis Anterior
Peroneus Brevis
Peroneus Longus
Peroneus Tertius
Extensor Digitorum Longus
Extensor Hallucis Longus

References

- Abramov, I. P., Stoklitsky, A. Y., Barer, A. S., & Filipenkov, S. N. (1994). Essential aspects of space suit operating pressure trade-off. *SAE Transactions*, 103(Section 1: Journal of Aerospace), 716-724.
- Aftab, Z., & Ali, A. (2017). Simulating a wearable lower-body exoskeleton device for torque and power estimation. In *IEEE-RAS international conference on humanoid robots*.
- Anderson, A. (2011). *Addressing design challenges in mechanical counterpressure spacesuit design and space-inspired informal education policy* (Master's Thesis). Massachusetts Institute of Technology, Department of Aeronautics and Astronautics.
- Anderson, A. (2014). *Understanding human-space suit interaction to prevent injury during extravehicular activity* (PhD Dissertation). Massachusetts Institute of Technology, Department of Aeronautics and Astronautics.
- Anderson, A., Hilbert, A., Bertrand, P., McFarland, S., & Newman, D. J. (2014). In-suit sensor systems for characterizing human-space suit interaction. In *44th international conference on environmental systems proceedings*.
- Anderson, A., Newman, D. J., & Welsch, R. E. (2015). Statistical evaluation of causal factors associated with astronaut shoulder injury in space suits. *Aerospace Medicine and Human Performance*, 86(7).
- Annis, J. F., & Webb, P. (2004). *Development of a space activity* (Tech. Rep.). NASA. (NASA CR-1892)
- Asbeck, A. T., Schmidt, K., Galiana, I., Wagner, D., & Walsh, C. J. (2015). Multi-joint soft exosuit for gait assistance. In *IEEE international conference on robotics and automation (icra) proceedings*.
- Benson, E., & Rajulu, S. (2009). Complexity of sizing for space suit applications. In *International conference on digital human modeling*.
- Bertrand, P., Reyes, S., & Newman, D. (2016). Pressure and kinematic in-suit sensors: assessing human-suit interaction for injury risk mitigation. In *IEEE aerospace conference proceedings*.
- Blickhan, R. (1989). The spring-mass model for running and hopping. *Journal of Biomechanics*, 22(11/12), 1217-1227.
- Carr, C. E., & Newman, D. J. (2007, December). Space suit bioenergetics: cost of transport during walking and running. *Aviation Space and Environmental Medicine*, 78(12), 1093-1102.
- Carr, C. E., & Newman, D. J. (2008). Characterization of a lower-body exoskeleton

- for simulation of space-suited locomotion. *Acta Astronautica*, 62(4-5), 308-323.
- Carr, C. E., & Newman, D. J. (2017). Exoskeleton energetics: Implications for planetary extravehicular activity. In *IEEE aerospace conference proceedings*.
- Carr, C. E., & Trevino, L. (2019). A first-order design requirement to prevent edema in mechanical counter-pressure space suit garments. *bioRxiv*.
- Cullinane, C. R., Rhodes, R. A., & Stirling, L. A. (2017). Mobility and agility during locomotion in the Mark iii space suit. *Aerospace Medicine and Human Performance*, 88(6), 589-596.
- Dainese. (2019). *Dainese returns to space to revolutionize astronaut safety*. <https://www.dainese.com/us/en/technology-innovation/space-suits.html>.
- Delp, S. L., Loan, J. P., Hoy, M. G., Zajac, F. E., Topp, E. L., & Rosen, J. M. (1990). An interactive graphics-based model of the lower extremity to study orthopaedic surgical procedures. *IEEE Transactions on Biomedical Engineering*, 37(8), 757-767.
- Diaz, A., Anderson, A., Kracik, M., Trotti, G., Hoffmann, J., & Newman, D. (2012). Development of a comprehensive astronaut spacesuit injury database. In *63rd international astronautical congress proceedings*.
- Diaz, A., & Newman, D. (2014). Musculoskeletal human-spacesuit interaction model. In *IEEE aerospace conference proceedings*.
- Diaz-Artiles, A., Shepherd, R., Kluis, L., Keller, N., Bai, H., Iyengar, N., & Audirsch, C. (2020). *SmartSuit: Hybrid, intelligent, and highly mobile EVA spacesuit for next generation exploration missions* (Tech. Rep.). NASA. (NASA Innovative Advanced Concepts (NIAC) - Phase I Final Report)
- Dionne, S. (1991). *Ax-5 mk iii, and shuttle space suit comparison test summary* (Tech. Rep.). NASA. (EVA Technical Document 91-SAE/SD-004)
- Dugan, S. A., & Bhat, K. P. (2005). Biomechanics and analysis of running gait. *Physical Medicine and Rehabilitation Clinics of North America*, 16, 603-362.
- Ferrati, F., Bortoletto, R., & Pagello., E. (2013). Virtual modelling of a real exoskeleton constrained to a human musculoskeletal model. In *Living machines proceedings*.
- Gernhardt, M. L., Jones, J. A., Scheuring, R. A., Abercromby, A. F., Tuxhorn, J. A., & Norcross, J. R. (2009, January). *Risk of compromised EVA performance and crew health due to inadequate EVA suit systems* (Human Research Program Requirements Document, HRP-47052, Rev. C). NASA.
- H.Gray. (1913). *Henry gray's anatomy: Descriptive and applied*. Philadelphia: Lea & Febiger.
- Holschuh, B., Obropta, E., Buechley, L., & Newman, D. J. (2012). Materials and textile architecture analyses for mechanical counter-pressure space suits using active materials. In *Aiaa space 2012 conference and exposition proceedings*.
- Iberall, A. S. (1964). *The use of lines of nonextension to improve mobility in full-pressure suits* (Tech. Rep.). Aerospace Medical Research Laboratories.
- Jackson, R. W., Dembia, C. L., Delp, S. L., & Collins, S. H. (2017). Muscle-tendon mechanics explain unexpected effects of exoskeleton assistance on metabolic rate during walking. *Journal of Experimental Biology*, 220(11), 2082-2095.
- Johnston, R. S. (1967). The development of space suit systems. In *Second interna-*

- tional symposium on basic environmental problems of man in space proceedings.*
- Judnick, D., Newman, D., & Hoffman, J. (2010). Modeling and testing of a mechanical counterpressure bio-suit system. *SAE Technical Papers*.
- Karavas, N. C., Tsagarakis, N. G., & Caldwell, D. G. (2012). Design, modeling and control of a series elastic actuator for an assistive knee exoskeleton. In *Proceedings of the IEEE RAS and EMBS international conference on biomedical robotics and biomechatronics*.
- Kerdok, A. E., Biewener, A. A., McMahon, T. A., Weyand, P. G., & Herr, H. M. (2002). Energetics and mechanics of human running on surfaces of different stiffnesses. *The American Physiological Society*, 92, 469-478.
- Kluis, L., Keller, N., Bai, H., Iyengar, N., Shepherd, R., & Diaz-Artiles, A. (2020). Modeling robotic actuation in the spacesuit during planetary ambulation. *Aerospace Medicine and Human Performance*. (Pending)
- Kracik, M., Meyen, F., Trotti, G., & Newman, D. J. (2012). The development of a high mobility space suit helmet for planetary exploration. In *63rd international astronautical congress*.
- Lee, S., Karavas, N., Qunlivan, B. T., Ryan, D. L., Perry, D., Eckert-Erdheim, A., ... Walsh, C. J. (2018). Autonomous multi-joint soft exosuit for assistance with walking overground. In *IEEE international conference on robotics and automation (icra) proceedings*.
- Leth, A., Hicks, J. L., Uchida, T. K., Habib, A., Dembia, C. L., Dunne, J. J., ... Delp, S. L. (2018). Opensim: Simulating musculoskeletal dynamics and neuromuscular control to study human and animal movement. *PLoS Computational Biology*, 14(7), 914-923.
- Li, H., Jin, Y., & Wang, C. (2012). Modeling and simulation of astronaut motions during extravehicular activity: a complex system based method. *AASRI Conference on Modeling, Identification and Control Modeling*, 3, 118-126.
- Li, J., Ye, Q., Ding, L., & Liao, Q. (2017). Modeling and dynamic simulation of astronaut's upper limb motions considering counter torques generated by the space suit. *Computer Methods in Biomechanics and Biomedical Engineering*, 20(9), 929-940.
- Manns, P., Sreenivassa, M., Millard, M., & Mombaur, K. (2017). Motion optimization and parameter identification for a human and lower back exoskeleton model. In *IEEE robotics and automation letters*.
- McFarland, S. (2016). Z-2 space suit: A case study in human spaceflight public outreach. In *S46th international conference on environmental systems proceedings*.
- McMahon, T. A. (1984). Muscles, reflexes, and locomotion. Princeton University Press.
- McMahon, T. A., & Cheng, G. C. (1990). The mechanics of running: How does stiffness couple with speed? *Journal of Biomechanics*, 23, 65-78.
- McMann, H. J., & McBarron, J. W. (1985). *Challenges in the development of the shuttle extravehicular mobility unit* (Tech. Rep.). NASA.
- Meyen, F. E. (2013). *Engineering a robotic exoskeleton for space suit simulation* (Master's Thesis). Massachusetts Institute of Technology, Department of Aeronautics and Astronautics.

- Morgan, D. A., Wilmington, R. P., Maida, J. C., & Demel, K. J. (1996). *Comparison of extravehicular mobility unit (EMU) suited and unsuited isolated joint strength measurements* (Tech. Rep.). NASA. (NASA Technical Paper 3613)
- NASA. (n.d.). *The space shuttle extravehicular mobility unit (emu)*. Suited for Spacewalking: An Activity Guide for Technology Education, Mathematics, and Science.
- NASA. (2011). *JSC human spaceflight capabilities - human health and performance*. nasa.gov.
- NASA. (2013, June). *Apollo - july 1969*. NASA Spacesuit Gallery.
- NASA. (2014, May). *Space station spacesuit image gallery*. NASA Spacesuit Gallery.
- NASA. (2017, April). *NASA's management and development of spacesuits*. Office of Inspector General.
- NASA. (2020). *Lsda hardware - partial gravity simulator (pogo)*. Lsda.jsc.nasa.gov.
- NASM. (2015). *Knee biomechanics: What is "screw home" rotation?* National Academy of Sports Medicine - <https://blog.nasm.org/uncategorized/knee-biomechanics-screw-home-rotation/>.
- Newman, D. J., Canina, M., & Trotti, G. L. (2007). Revolutionary design for astronaut exploration-beyond the bio-suit system. In *Aip conference proceedings*.
- Newman, D. J., Hoffman, J., Bethke, K., Carr, C., Jordan, N., Sim, L., . . . Trotti, G. (2005). *Astronaut bio-suit system for exploration class missions* (Tech. Rep.). NASA. (NIAC PHASE II FINAL REPORT)
- Newman, D. J., Schmidt, P. B., & Rahn, D. B. (2000). Modeling the extravehicular mobility unit (EMU) space suit: physiological implications for extravehicular activity (EVA). *SAE Technical Papers*(724).
- Newman, D. J., & Wessendorf, A. M. (2015). *System and method for measuring skin movement and strain and related techniques*. Patent No.: US 9,149,224 B1.
- Nisell, R., Nemeth, G., & Ohlsen, H. (1986). Joint forces in extension of the knee: Analysis of a mechanical model. *Acta Orthopaedica*, 57(1), 41-46.
- Norcross, J. R., & Clowers, K. (2010, June). *Metabolic costs and biomechanics of level ambulation in a planetary suit* (TP-2010-216115). NASA.
- Norcross, J. R., Lee, L. R., Clowers, K. G., Morency, R. M., Desantis, L., DeWitt, J. K., . . . Gernhardt, M. L. (2009). *Feasibility of performing a suited 10-km ambulation on the moon - final report of the EVA Walkback Test (EWT)* (Tech. Rep.). NASA. (NASA TP-2009-214796)
- Obropta, E. W. (2015). *On the deformation of human skin for mechanical counter pressure space suit development* (Master's Thesis). Massachusetts Institute of Technology, Department of Aeronautics and Astronautics.
- Obropta, E. W., & Newman, D. J. (2015). A comparison of human skin strain fields of the elbow joint for mechanical counter pressure space suit development. In *IEEE aerospace conference proceedings*.
- Obropta, E. W., & Newman, D. J. (2016). Skin strain fields at the shoulder joint for mechanical counter pressure space suit development. In *IEEE aerospace conference proceedings*.
- Opperman, R. A., Waldie, J. M. A., Natapoff, A., Newman, D. J., & Jones, J. A. (2010, October). Probability of spacesuit-induced fingernail trauma is associated

- with hand circumference. *Aviation Space and Environmental Medicine*, 81(10), 907-913.
- Porter, A. P., Marchesini, B., Potryasilova, I., Rossetto, E., & Newman, D. J. (2020). Soft exoskeleton knee prototype for advanced space suits and planetary exploration. In *IEEE aerospace conference*. (Pending)
- Quinlivan, B., Lee, S., Rossi, D. M., Grimmer, M., Siviyy, C., Karavas, N., . . . Walsh, C. (2017). Assistance magnitude versus metabolic cost reductions for a tethered multiarticular soft exosuit. *Science Robotics*, 2(2).
- Rader, A. A., Newman, D. J., & Carr, C. E. (2007). Loping: a strategy for reduced gravity human locomotion? *SAE Technical Papers*(724).
- Reid, C., Harvill, L., England, S., Young, K., Norcross, J., & Rajulu, S. (2014). An ergonomic evaluation of the extravehicular mobility unit (EMU) space suit hard upper torso (HUT) size effect on metabolic, mobility, and strength performance. In *Human factors and ergonomics society's international annual meeting proceedings*.
- Roberts, J. (2015, August). *NASA's next prototype spacesuit has a brand new look*. <https://www.nasa.gov/content/nasa-s-next-prototype-spacesuit-has-a-brand-new-look-and-it-s-all-thanks-to-you>.
- Rodriggs, L. (2017). *xemu lite development plan*. NASA.
- Ronco, L. (2014). *Protection device*. Patent No.: US 2014/0110924 A1.
- Sawicki, G. S., Beck, O. N., Kang, I., & Young, A. J. (2020). The exoskeleton expansion: improving walking and running economy. *Journal of NeuroEngineering and Rehabilitation*, 17(1), 1-9.
- Sawicki, G. S., & Khan, N. S. (2016). A simple model to estimate plantarflexor muscle-tendon mechanics and energetics during walking with elastic ankle exoskeletons. *IEEE Transactions on Biomedical Engineering*, 63(5), 914-923.
- Schaffner, G., Newman, D. J., & Robinson, S. K. (2000). Computational simulation of extravehicular activity dynamics during a satellite capture attempt. *Journal of Guidance, Control, and Dynamics*, 23(2), 367-369.
- Schmidt, P., Newman, D., & Hodgson, E. (2001). Modeling space suit mobility: Applications to design and operations. *SAE Technical Papers*.
- Schmidt, P. B. (2011). *An investigation of space suit mobility with applications to EVA operations* (Master's Thesis). Massachusetts Institute of Technology, Department of Aeronautics and Astronautics.
- Schwartz, M. H., Rozumalski, A., & Trost, J. P. (2008). The effect of walking speed on the gait of typically developing children. *Journal of Biomechanics*, 41(8), 1639-1650.
- SimTK. (2020a). *Gait 2392 and 2354 models - opensim documentation*. <https://simtk-confluence.stanford.edu>.
- SimTK. (2020b). *Getting started with inverse dynamics - opensim documentation*. <https://simtk-confluence.stanford.edu>.
- SimTK. (2020c). *Getting started with inverse kinematics - opensim documentation*. <https://simtk-confluence.stanford.edu>.
- SimTK. (2020d). *Getting started with rra - opensim documentation*. <https://simtk-confluence.stanford.edu>.

- SimTK. (2020e). *Probes - opensim documentation*. <https://simtk-confluence.stanford.edu>.
- SimTK. (2020f). *Simulation-based design to reduce metabolic cost - opensim documentation*. <https://simtk-confluence.stanford.edu/display/OpenSim/Simulation-Based+Design+to+Reduce+Metabolic+Cost>.
- Skoog, A. I., & Abramov, I. P. (1986, February). The Soviet/Russian spacesuit history. Part iii-the European connection. *Acta Astronautica*, *41*(12), 1002-1014.
- Skoog, A. I., Abramov, I. P., Stoklitsky, A. Y., & Doodnik, M. N. (2002). The Soviet-Russian space suits: A historical overview of the 1960's. *Acta Astronautica*, *51*(1-9), 113-131.
- Stirling, L., Arezes, P., & Anderson, A. (2019). Implications of space suit injury risk for developing computational performance models. *Aerospace Medicine and Human Performance*, *90*(6), 553-565.
- Strauss, S. (2004). *Extravehicular mobility unit training suit symptom study report* (Tech. Rep.). NASA.
- Strauss, S., Krog, R. L., & Feiveson, A. H. (2005, May). Extravehicular mobility unit training and astronaut injuries. *Aviation Space and Environmental Medicine*, *76*(5), 469-474.
- Stroming, J. P. (2020). *Design and evaluation of elements of a life support system for mechanical counterpressure spacesuits* (Master's Thesis). Massachusetts Institute of Technology, Department of Aeronautics and Astronautics.
- Thomas, K. S. (2016, August). *Intra-extra vehicular activity (IEVA) Russian and Gemini*. JSC/EC5 Spacesuit Knowledge Capture (KC) Series.
- Umberger, B. R. (2003). Stance and swing phase costs in human walking. *Journal of the Royal Society*, *7*(50), 1329-1340.
- Umberger, B. R., Gerritsen, G. M., & Martin, P. E. (2003). A model of human muscle energy expenditure a model of human muscle energy expenditure. *Computer Methods in Biomechanics and Biomedical Engineering*, *6*(2), 99-111.
- Waldie, J. M. A. (2005a). *Mechanical counter pressure space suits: Advantages, limitations and concepts for Martian exploration*. The Mars Society.
- Waldie, J. M. A. (2005b). *The viability of mechanical counter pressure space suits* (PhD Dissertation). Royal Melbourne Institute of Technology, Department of Aerospace, Mechanical and Manufacturing Engineering.
- Wehner, M., Quinlivan, B., Aubin, P. M., Martinez-Villalpando, E., Baumann, M., Stirling, L., ... Walsh, C. (2013). A lightweight soft exosuit for gait assistance. In *IEEE international conference on robotics and automation (icra) proceedings*.
- Wessendorf, A. M., & Newman, D. J. (2012). Dynamic understanding of human-skin movement and strain-field analysis. *IEEE Transactions on Biomedical Engineering*, *59*(12), 3432-3438.
- Williams, D. R., & Johnson, B. J. (2019). *EMU shoulder injury tiger team report* (Tech. Rep.). NASA.
- Yamaguchi, G. T., & Zajac, F. E. (1989). A planar model of the knee joint to characterize the knee extensor mechanism. *Journal of Biomechanics*, *22*(1).

Zhu, Y., Zhang, G., Zhang, C., Liu, G., & Zhao, J. (2015). Biomechanical modeling and load-carrying simulation of lower limb exoskeleton. *Bio-Medical Materials and Engineering*, 26(2), S729-S738.